ARL

The University of Texas at Austin

TECHNICAL REPORT

ARL-TR-96-2
11 January 1996

Copy Number 29

Evaluation of the Dominant Mode Rejection Beamformer

Technical Report under Contract N00039-91-C-0082

TD No. 01A2073, Acoustics and Engineering Analysis for ADS II

Tina R. Messerschmitt

Prepared for: Space and Naval Warfare Systems Command
Department of the Navy • Arlington, VA 22245-5200

Applied Research Laboratories•The University of Texas at Austin•Post Office Box 8029•Austin, Texas 78713-8029

DISCLAIMER NOTICE

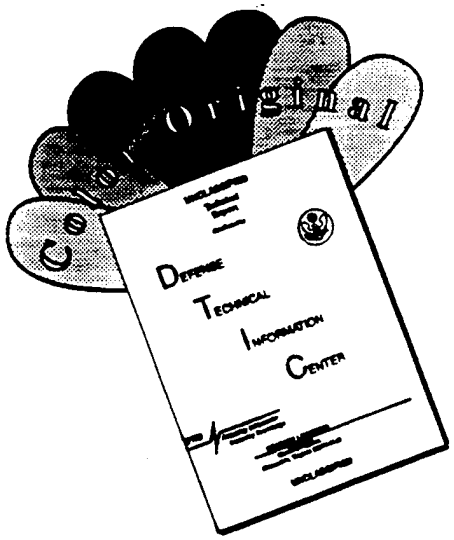

THIS DOCUMENT IS BEST QUALITY AVAILABLE. THE COPY FURNISHED TO DTIC CONTAINED A SIGNIFICANT NUMBER OF COLOR PAGES WHICH DO NOT REPRODUCE LEGIBLY ON BLACK AND WHITE MICROFICHE.

REPORT DOCUMENTATION PAGE

Form Approved
OMB No. 0704-0188

1. AGENCY USE ONLY (Leave blank)	2. REPORT DATE	3. REPORT TYPE AND DATES COVERED
	11 Jan 96	technical

4. TITLE AND SUBTITLE
Evaluation of the Dominant Mode Rejection Beamformer, Technical Report under Contract N00039-91-C-0082, TD No. 01A2073, Acoustics and Engineering Analysis for ADS II

5. FUNDING NUMBERS
N00039-91-C-0082,
TD No. 01A2073

6. AUTHOR(S)
Messerschmitt, Tina R.

7. PERFORMING ORGANIZATION NAMES(S) AND ADDRESS(ES)
Applied Research Laboratories
The University of Texas at Austin
P.O. Box 8029
Austin, Texas 78713-8029

8. PERFORMING ORGANIZATION REPORT NUMBER
ARL-TR-96-2

9. SPONSORING/MONITORING AGENCY NAME(S) AND ADDRESS(ES)
Space and Naval Warfare Systems Command
Department of the Navy
Arlington, VA 22245-5200

10. SPONSORING/MONITORING AGENCY REPORT NUMBER

11. SUPPLEMENTARY NOTES

12a. DISTRIBUTION/AVAILABILITY STATEMENT
Approved for public release; distribution is unlimited.

12b. DISTRIBUTION CODE

13. ABSTRACT (Maximum 200 words)
(see reverse side)

14. SUBJECT TERMS
adaptive beamforming
integration time
reduced rank estimation

15. NUMBER OF PAGES
95

16. PRICE CODE

17. SECURITY CLASSIFICATION OF REPORT	18. SECURITY CLASSIFICATION OF THIS PAGE	19. SECURITY CLASSIFICATION OF ABSTRACT	20. LIMITATION OF ABSTRACT
UNCLASSIFIED	UNCLASSIFIED	UNCLASSIFIED	SAR

NSN 7540-01-280-5500

Standard Form 298 (Rev. 2-89)
Prescribed by ANSI Std. 239-18
298-102

13. (cont'd)

Increasing the number of hydrophones in an array should increase beamformer performance. However, when the number of hydrophones is large, integration times must be long enough to give accurate cross-spectral matrix (CSM) estimates, but short enough so that the dynamic behavior of the noise described by the CSM is captured. The dominant mode rejection (DMR) beamformer calculates adaptive weights based on a reduced rank CSM estimate, where the CSM estimate is formed with a subset of the largest eigenvalues and their eigenvectors. Since the largest eigenvalue/eigenvector pairs are estimated rapidly, the integration time required is reduced. The purpose of this study was to examine the DMR beamformer performance using several bottom-mounted horizontal line arrays, in both deep and shallow water environments. The data were processed with two fully adaptive beamformers and the DMR beamformer. The DMR beamformer showed less output power bias at shorter integration times and also showed better performance than the fully adaptive beamformers when using arrays with larger numbers of hydrophones. Thus, in highly dynamic noise environments, the DMR beamformer may be a more appropriate implementation to use for passive sonar detection systems.

ACKNOWLEDGMENTS

I would like to thank Richard Gramann for his guidance and advice during this work. I would also like to express my gratitude to Clark Penrod and Professor Alan Bovik for serving on my committee. I would like to thank my mother and father for their constant support and encouragement. I also appreciate the love and understanding I received from my sister, Tracy, and my fiancé, Bheeshmar. Finally, I would like to thank Dante for his continued assistance.

This work was sponsored by the U.S. Naval Space and Naval Warfare Systems Command, under the technical direction of CAPT William Hatcher and Mr. J. P. Feuillet. This source of support is gratefully acknowledged.

November 1995

This page intentionally left blank.

TABLE OF CONTENTS

LIST OF TABLES

This page intentionally left blank.

LIST OF FIGURES

PREFACE

This material was originally published in December 1995 as a thesis, in partial fulfillment of the requirement for the degree of Master of Science in Engineering, The University of Texas at Austin.

This page intentionally left blank.

1. INTRODUCTION

Many passive sonar systems rely on adaptive beamforming to provide gain against interfering signals. The adaptive beamformer places nulls in the directions of interferers and allows the gain of the array to be many times that achieved with conventional, or delay and sum, beamforming (CBF). This additional gain can be important in high noise environments, where many loud interferers are present. In particular, many shallow water environments can be characterized as high noise, due to shipping traffic. Also, the noise environment can be classified as highly dynamic, due to the high bearing rates seen on many interfering traces, as the dominant interferers are generally in close proximity to the array. Thus, the ability of the adaptive beamformer to adapt to this environment and suppress interferers in the sidelobe region is critical to the performance of a system in such an environment.

Another way the gain of the array can be increased is by increasing the number of hydrophones in the array. Most of the recent studies performed at ARL:UT have used arrays with 8 or 16 hydrophones. These studies have shown that due to directional noise fields in shallow water areas, arrays with 16 hydrophones achieve 4 to 5 dB of gain over arrays with 8 hydrophones. The next logical question is whether a 32 hydrophone array can achieve another 4 to 5 dB of gain. This is important because in a cylindrical spreading type propagation environment, a 3 dB increase in gain can double the detection range of the processor.

However, there are potential drawbacks to increasing the number of hydrophones. First, the computational burden increases as the number of hydrophones increases. A general rule of thumb is that inverting the cross-spectral matrix (CSM)

is an $O(N^3)$ operation, where N is the number of hydrophones. Also, the integration time required to obtain an adequate estimate of the CSM increases as the number of hydrophones increases. Increasing the integration time of the CSM may not be practical for a number of reasons. Thus, the following discussion provides the rules for obtaining an adequate CSM estimate, the steps for computing the CSMs, and the reasons that increasing the integration time of the CSM may be impractical.

1.1 CSM INTEGRATION TIME REQUIREMENTS

In order to place nulls in the direction of the interferers, the beamformer requires information on the noise environment. The source of this information is the cross-spectral matrix. An estimate of the CSM is formed by averaging several single CSM samples. Each CSM sample is calculated by averaging several FFT frequency bins and multiplying each channel's "band-averaged FFT" bin by the other channels' corresponding FFT bins. This operation forms a single CSM sample with a specified bandwidth. Several of these CSM samples are then averaged to obtain a specified CSM integration time.

Clearly, the integration time must be short enough so that the dynamic behavior of the noise is captured and the noise described by the CSM can be considered somewhat stationary. Also, the bandwidth of the CSM must be small enough to avoid mismatch in the adaptive weights (due to the bandwidth being too large relative to the center frequency), to avoid phase errors across the array, and to adequately describe the variation in the noise field seen at closely spaced frequencies. Thus both the integration time and bandwidth must be kept to a minimum so that the dynamic noise environment can be adequately described.

The accuracy of the information provided to the beamforming algorithm (through the CSM) determines how well the beamformer can null out the interfering signals and allow the desired signal to pass without attenuation or distortion. The accuracy of the CSM estimate is directly proportional to the integration time and the CSM bandwidth. Hence, an inherent conflict arises between capturing the dynamics of the noise field and obtaining an accurate estimate of the CSM.

In a previous study, Grant et al.[1] examined the bias obtained in the beamformer output power when using an estimate of the CSM that contains few samples (either time or frequency). They expanded on the work of Capon and Goodman[2] to show that the output power of the beamformer would be biased when using CSMs that do not have sufficient averaging. The expression they derived, shown below, shows that the accuracy of the minimum variance distortionless response (MVDR) beamformer output power estimate is proportional to the number of samples used to calculate the CSM. The estimated MVDR beamformer output power is

$$E\left\{\hat{P}_o\right\} = \frac{N_s - N + 1}{N_s} P_o \,, \tag{1.1}$$

where N is the number of sensors described in the CSM, N_s is the number of snapshots used to calculate the CSM estimate, P_o is the output power obtained with the actual CSM, and $\hat{P}_o$ is the MVDR output power estimated using the estimated CSM. In Grant et al.'s terminology, a snapshot is referred to as a single frequency bin for one FFT. Averaging can be done in time (by averaging bins from successive FFTs) or in frequency. Hence, a CSM formed with three FFT frequency bin averages (i.e., n_{bin} = 3) to obtain a specified bandwidth, and seven time averages (n_{fft} = 7), would be composed of 21 snapshots (N_s = 21).

At ARL:UT, the timeseries data are windowed using a Hanning window before calculating the FFT. Also, the FFTs are generally overlapped in time by

50% (i.e., the next FFT in the series contains only 50% new timeseries data). Accounting for these effects gives the following relation for the number of effective snapshots, when n_{fft} and n_{bin} are greater than one:

$$N_s' = 0.56 n_{fft} n_{bin} = 0.56 N_s. \tag{1.2}$$

If n_{fft}=1, then the expression is $N_s' = 0.67 N_s$.

Equation (1.1) can be used to derive an equation for the minimum number of snapshots required to limit the beam noise loss to 1 dB. Given a specified bandwidth, the minimum integration time for 1 dB of beam noise loss is

$$T = \frac{1}{\Delta f} Ns' \geq \frac{1}{\Delta f}\left(\frac{N-1}{0.21}\right), \tag{1.3}$$

where Δf is the bandwidth of the CSM. Figure 1.1 shows the integration time required to maintain less than 1 dB of output power bias as a function of the number of hydrophones and the CSM bandwidth from Eq. (1.3). Notice that the minimum integration time is a linear function of the number of hydrophones. It is clear from Fig. 1.1 that several minutes of integration time may be necessary to keep the output power bias to reasonable levels, particularly for arrays with 32 hydrophones or more.

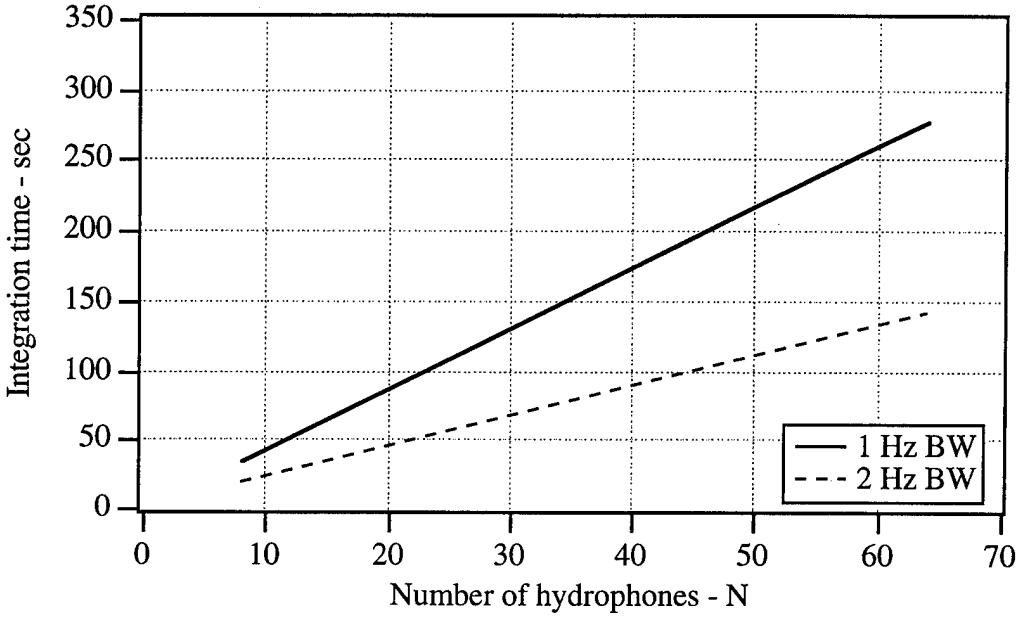

Figure 1.1 Integration time required for beam noise loss of 1 dB.

AS-96-2

The bandwidth of the CSM must also be constrained to avoid phase errors across the array. This constraint is based on the phase difference

$$\Delta\phi = 2\pi\frac{L}{\lambda_1} - 2\pi\frac{L}{\lambda_2}, \tag{1.4}$$

where λ_1 and λ_2 are the wavelengths at the upper and lower band edges and L is the length of the array. Rearranging and using $f = c/\lambda$ and $f_1 - f_2 = \Delta f$ gives

$$\Delta\phi = 2\pi\frac{L}{c}\Delta f, \tag{1.5}$$

where c is the speed of sound and Δf is the bandwidth. A common requirement is that the phase difference be less than one-tenth of a cycle, or $\Delta\phi < 2\pi/10$. Thus

$$\Delta f < \frac{c}{10L}. \tag{1.6}$$

If this constraint is not met, the bandwidth over which the steering vector is being applied is large enough that the error at the band edges can cause mismatch between the steering vector and the vector pointing in the direction of the signal. This will result in signal suppression and decreased beamformer performance.

Equation (1.6) sets a constraint on the bandwidth of the CSM based on the length of the array. This constraint can be combined with Eq. (1.3) to show the total integration time required for a given number of hydrophones. Assuming that the array length is proportional to the number of hydrophones that are uniformly spaced at a fraction of the wavelength, or

$$L = (N-1)\frac{\lambda}{k}, \tag{1.7}$$

Eq. (1.6) becomes

$$\Delta f < \frac{ck}{10\lambda(N-1)}, \tag{1.8}$$

where k is the proportionality constant that defines the hydrophone spacing with respect to the wavelength. Thus, Eq. (1.3) becomes

$$T \geq \left(\frac{10\lambda(N-1)}{ck}\right)\left(\frac{N-1}{0.21}\right) = 47.6\frac{\lambda}{ck}\left(N^2 - 2N + 1\right). \tag{1.9}$$

Figure 1.2 shows the minimum integration time from Eq. (1.9), assuming that k = 2.0, λ = 10.0 m, and c = 1500 m/s. It is clear from Fig. 1.2 that the minimum integration time of the CSM is no longer a linear function of the number of hydrophones. When the array length is proportional to the number of hydrophones, the maximum bandwidth of the CSM is inversely proportional to the number of hydrophones, from Eq. (1.6). Also, the minimum number of snapshots required to keep the beam noise bias to 1 dB is directly proportional to the number of hydro-

phones. Therefore, the integration time of the CSM is proportional to the number of hydrophones squared. Thus, Fig. 1.2 shows a quadratic relationship between the integration time of the CSM and the number of hydrophones.

Figure 1.2 shows that more than 2 minutes of integration time may be necessary for arrays with 32 hydrophones when processed with an adaptive beamformer. Thus an alternative beamforming algorithm may be necessary for arrays with many sensors that are placed in dynamic noise environments.

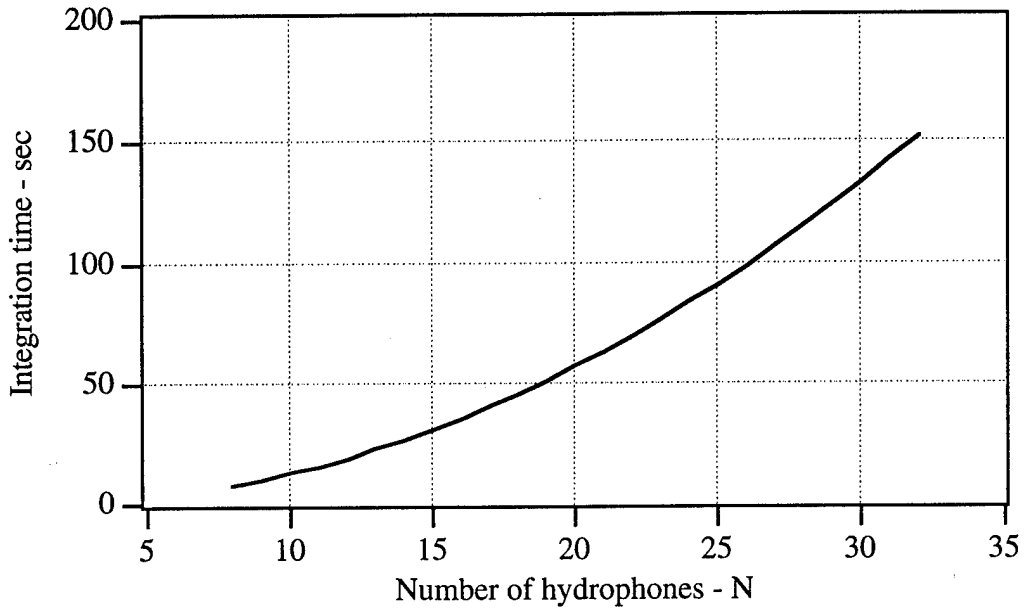

Figure 1.2 Minimum integration time using the CSM bandwidth constraint in Eq. (1.6).

AS-96-3

1.2 THE DOMINANT MODE REJECTION BEAMFORMER

The dominant mode rejection (DMR) beamformer was described by Abraham and Owsley in Ref. 3. This beamformer calculates adaptive weights based on a reduced rank CSM estimate, where the CSM estimate is formed with the D largest eigenvalues, corresponding in general to the D dominant sources in the noise

field. Thus the adaptive weights respond to the loudest sources in the noise field. More importantly, the integration time or amount of data required to obtain this CSM estimate is reduced, as the largest eigenvalue/eigenvector pairs are estimated much more rapidly than the smaller ones. Thus the ability to calculate weights using less data will exist, allowing the adaptive beamformer to adapt more rapidly to the dynamic noise environment and possibly improving the ABF performance. For example, if a fully adaptive beamformer is used with 30 hydrophones, approximately 130 sec of data are needed to obtain an accurate estimate of the CSM from Fig. 1.2. However, if the DMR beamformer is used with the same 30 hydrophone array, but with only 15 eigenvalues, approximately 30 sec of integration time (one-fourth the integration time for the fully adaptive beamformer) are needed. Thus the ability of the beamformer to respond to the dynamics of the noise environment is enhanced.

The purpose of this study was to examine the performance of the dominant mode rejection beamformer in a real ocean environment and to determine whether performance comparable to a fully adaptive beamformer could be achieved. A comparison of the output power bias obtained with DMR and fully adaptive ABF is provided. Also, the performance gain obtained by increasing the number of hydrophones and the performance degradation from increasing the integration time of the CSM is evaluated. Finally, the DMR beamformer's performance using CSMs with shorter integration times is evaluated. In order to address these issues, the DMR algorithm was coded, and a sensitivity study of its performance conducted. Finally, data were processed from three ocean environments, and the performance of the DMR beamformer was compared directly to a fully adaptive algorithm. The following sections describe the dominant mode rejection beamformer, the fully adaptive algorithms used at ARL:UT and the data used for this evaluation, and they discuss the results of this study.

2. HISTORICAL PERSPECTIVE

The study of adaptive beamforming for sonar arrays began in the 1960's. These studies converged on an optimal processor that uses the measured correlation characteristics from the hydrophones to provide gain against interfering signals.[4] The adaptive beamformer provides gain by creating nulls in the direction of the loud interferers in the environment described by the CSM. This is accomplished by calculating a set of complex weights that, when applied to the hydrophone outputs, will give unity gain in the look direction while minimizing the output power. The output power of the beamformer is

$$P = w^H R w \,, \tag{2.1}$$

where w is the weight vector, R is the CSM, and H indicates complex conjugate, or Hermitian, transpose. The goal is to minimize the output power subject to the look direction constraint, or

$$\min(w^H R w) \text{ subject to } w^H d = 1 \,, \tag{2.2}$$

where d is the look direction steering vector which describes the expected spatial properties of the desired signal.

Using Lagrange multipliers gives the solution for the MVDR weights to be

$$w = \frac{R^{-1} d}{d^H R^{-1} d} \,. \tag{2.3}$$

When the information supplied to the beamformer is inaccurate, due to hydrophone location errors, calibration errors, or signal multipath, mismatch between the received signal and the steering vector occurs. As a result, the beam-

former may treat the desired signal as an interfering signal. Thus, depending on the SNR, the desired signal could be suppressed in minimizing the output power. Cox et al.[4] described a robust adaptive beamformer in Ref. 4 that limits this signal suppression. They noticed that many of these errors affect the beamformer in a way similar to adding spatially uncorrelated noise to each hydrophone. Therefore, if the beamformer can limit the array gain against white noise (white noise gain, or G_w), the errors would be reduced. Thus, the white noise gain is a measure of the robustness of the beamformer. If the white noise gain is not constrained, the overall magnitude of the weight vectors can increase. Thus, small errors in the information supplied to the beamformer can cause large errors in the beamformer output.

The weights of the white noise gain constrained beamformer are derived by minimizing the output power subject to the look direction constraint and the white noise gain constraint, or

$$\min(w^H R w) \text{ subject to } w^H d = 1 \text{ and } G_w \geq \delta^2. \tag{2.4}$$

When a beamformer has unity gain in the look direction, the white noise gain is defined as

$$G_w = \frac{1}{w^H w}. \tag{2.5}$$

Again, Lagrangian methods are used to find the solution

$$w = \frac{(R+\varepsilon I)^{-1} d}{d^H (R+\varepsilon I)^{-1} d}, \tag{2.6}$$

where ε is the smallest positive value such that $G_w > \delta^2$ and εI is the white noise injected into the CSM. $G_w(\varepsilon)$ is a monotonic increasing function of ε, and $G_w(\infty) = N$, yielding the unshaded beamformer. It is clear that the implementation

of the white noise gain constrained beamformer involves simply adding ε to the diagonal of the CSM, which is the same as adding ε to each eigenvalue of the CSM.

Cox et al.[4] also presented an example that showed the effectiveness of the white noise gain constrained beamformer. The example illustrated the suppression of a strong signal on boresight when the actual hydrophone positions are different from the nominal hydrophone positions. Without the white noise gain constraint, the white noise gain was drastically reduced and the signal was severely suppressed. Using the white noise gain constrained beamformer, the white noise gain was maintained above a specified limit and the signal was not suppressed.

Gramann in Ref. 5 discusses the implementation of the white noise gain constrained adaptive beamformer (WNGC ABF) at ARL:UT. The white noise gain constraint is set relative to 10log$N$ and, in general, the constraint is set to 3 dB below 10log$N$. Thus, the white noise gain constraint equation is

$$G_w \geq 10\log N + wnc\,, \tag{2.7}$$

where $wnc = -3$ dB. Previous work has shown that this level of the constraint provides reasonable robustness against mismatch, while not overly penalizing the ability of the beamformer to suppress interferers in directions other than the look direction.

2.1 REDUCED-RANK BEAMFORMERS

The purpose of this study is to examine the dominant mode rejection beamformer, a reduced-rank beamformer. There are many other studies that have employed a reduced-rank form of beamforming. Most of these studies have used the largest eigenvalues of the CSM and the corresponding eigenvectors to deter-

mine the number or location of the sources in the environment described by the CSM. Kirsteins and Tufts[6] were interested in detecting signals when the signal-to-noise ratio (SNR) was low. Their algorithm defined a low rank matrix as one in which all the signals in the matrix can be written as a linear combination of r basis vectors, where r is less than the number of hydrophones in the array. They used the principal component inverse method to approximate the strong interferers in a low rank CSM. The strong interferers were subtracted from the observed data, and the desired signals were detected. They also developed an expression for the error when using a low rank matrix approximation. They used real and simulated examples to demonstrate the performance of the low rank approximation.

The goals of Kirsteins and Tufts' study were similar to the goals of this study. Both were interested in the problem of low SNR detection. However, the algorithms developed by Kirsteins and Tufts were unrelated to any of the algorithms previously used at ARL:UT. Conversely, the ABF algorithms used at ARL:UT could easily be modified to produce the dominant mode rejection beamformer developed by Abraham and Owsley.[3] Therefore, as a practical matter, the DMR beamformer was the better algorithm to begin examining reduced-rank beamforming for this study. Further work may involve a comparison of the DMR method with Kirsteins and Tufts' approach.

In another study using a reduced-rank beamformer, Johnson and DeGraaf[7] determined a way to increase the signal-to-noise ratio of an array for better bearing determination at the expense of array gain. Their method involved computing the energy in all possible beams from the eigenvalues and eigenvectors of the CSM given the number of sources. The peaks in this spectrum corresponded to the locations of the acoustic sources. The study showed that their reduced-rank method could achieve better bearing detection performance than the MUSIC[8] approach.

However, both their method and MUSIC are very sensitive to mismatch. This study is interested in beamforming algorithms that are somewhat robust to source mismatch. Hence, Johnson and DeGraaf's method is inappropriate for this study.

Other studies have developed reduced-rank methods for determining the number of sources in the noise field. Both Bienvenu and Kopp[9] and Chen et al.[10] developed such methods. These methods are based in the idea that given that there are N hydrophones in the array and p sources in the acoustic field, the smallest $N-p$ eigenvalues of the true CSM will be approximately equal. However, the $N-p$ smallest eigenvalues of the CSM estimated from the data will not be equal due to the stochastic noise process. Therefore, a threshold could be developed to estimate the value of $N-p$, and then p, the number of sources, could be calculated.

Bienvenu and Kopp[9] developed and discussed a test for the number of sources in the acoustic field based on the above statements. Their test did not require information about the wavefront shapes and depended only on the eigenvalues of the correlation matrix. Bienvenu and Kopp's study only described the test for the number of sources in the noise field. Bienvenu and Kopp did not include any experiments to verify their results.

Chen et al.[10] developed a similar test for detecting the number of sources present in the acoustic field. Their method involved finding an upper threshold for the value of the N–pth smallest eigenvalue. For each eigenvalue, starting with the smallest, a predicted upper threshold was calculated. The total number of eigenvalues that were less than the threshold determined the number of sources. The distinctive feature of their method was the parameter, t, which adjusted the performance of their detection scheme. Chen et al. discussed how to choose a value for t based on minimizing the probability of a detection error. Chen et al. conducted three simulations and computed the probability of detection error for

each simulation to illustrate the performance of their detection scheme. These simulations showed that the probability of a detection error was close to the theoretical value.

However, Abraham[11] noted that, unlike most other reduced-rank beamformers, the DMR beamformer does not need to know the exact number of sources. Only the number of dominant sources needs to be determined. This makes implementation of the DMR beamformer easier than implementation of other reduced-rank beamformers.

Kim and Un[12] developed a reduced-rank method to decrease the signal suppression caused by steering errors. They reduced the degrees of freedom of the beamformer so that the desired signal was not nulled when steering errors are present. This was accomplished by rotating the signal subspace defined by the largest eigenvalues of the covariance matrix to find a weight vector that was orthogonal to all of the interferers. They presented analytical and simulation results that proved the robustness of their method to steering errors using no interferers and one interferer. Kim and Un's study was important because it showed that robust beamforming was possible with a reduced rank beamformer.

It is clear that most of the studies to date involving reduced-rank methods have been trying to determine the number or location of the sources in the environment described by the CSM. However no studies have attempted to evaluate the performance of a reduced-rank beamformer using CSMs with reduced integration times. Currently, the WNGC beamformer provides the most gain against interferers; however the WNGC beamformer can require large CSM integration times which may over-average a dynamic noise field. Thus, it would be beneficial to find a beamformer that performs as well as the WNGC beamformer but allows the use of shorter CSM integration times. This study will investigate the dominant mode

rejection beamformer for low SNR detection using CSMs with reduced integration times.

2.2 THE DOMINANT MODE REJECTION BEAMFORMER

Abraham and Owsley developed a reduced-rank method of beamforming in Ref. 3. They rewrite the CSM in terms of its eigenvalues λ and eigenvectors *m:*

$$R = \sum_{i=1}^{N} \lambda_i m_i m_i^H . \tag{2.8}$$

The largest eigenvalues are associated with the loudest noise sources or dominant modes in the environment described by the CSM. Abraham and Owsley approximate the CSM using the D largest eigenvalues and their corresponding eigenvectors plus a noise term. The new reduced rank CSM estimate is

$$\hat{R} = e \sum_{i=1}^{D} \psi_i m_i m_i^H + \sigma^2 I_N , \tag{2.9}$$

where $\psi_i = \lambda_i - \sigma^2$ and e is a scalar enhancement factor.

Replacing R with $\hat{R}$ in the MVDR solution gives

$$\hat{w}(\theta) = \frac{d(\theta) - \sum_{i=1}^{D} \beta_i m_i m_i^H d(\theta)}{N - \sum_{i=1}^{D} \beta_i d(\theta)^H m_i m_i^H d(\theta)} , \tag{2.10}$$

where $\beta = \dfrac{1}{1 + \dfrac{\sigma^2}{e\psi}}$ and N is the number of hydrophones in the CSM.

In examining the form of Eq. (2.10), it is interesting to note that as e decreases to zero, β approaches zero, and the dominant mode rejection weights of Eq. (2.10) approach the unshaded conventional beamformer weights

$$w = \frac{d}{N} . \tag{2.11}$$

Since e is used as an "enhancement factor" for the eigenvalues (and thus controls emphasis of the information in the CSM) in the weights calculation, it is logical that, as the information on the noise field is removed from the weights calculation, the weights would approach the CBF solution. Further discussion of the sensitivity of the DMR beamformer to σ^2 and e is provided in Sections 4.4.1 and 4.4.2.

Substituting the unshaded conventional beamformer weights from Eq. (2.11) into the white noise gain formula in Eq. (2.5) shows that the unshaded conventional beamformer white noise gain values are constant and equal to the number of hydrophones, N. As mentioned above, the dominant mode rejection weights approach the unshaded conventional beamformer weights as e decreases; therefore, as later results verify, the dominant mode rejection white noise gain values should approach N as e decreases. In Section 4.4.2, e will be used to provide a measure of robustness control to the DMR beamformer.

After Abraham and Owsley[3] developed the dominant mode rejection beamformer, they compared the DMR and MVDR beamformers using one source, one interferer, and one dominant mode. This comparison suggested that more dominant modes were needed as the interferer level approached the signal level. This was because the interferer was no longer a dominant source; therefore the eigenvector corresponding to the largest eigenvalue no longer contained information only about the interferer. Abraham and Owsley suggested that using a dominant

mode for each strong plane wave interferer would allow the DMR beamformer to achieve the same gain against the interferers as the MVDR beamformer. One of the objectives of this study was to determine if DMR beamformer performance equivalent to MVDR beamformer performance could be achieved in a real ocean noise environment.

Abraham and Owsley also compared the numerical savings versus performance of the DMR beamformer using different methods for calculating the eigenvalues and eigenvectors of the CSM. A brute force method was used that computed all of the eigenvalues and eigenvectors. Also, two numerically faster methods that estimated only the D largest eigenvalues and their corresponding eigenvectors were used. The results showed that the performance of the quicker methods was acceptable but not equivalent to the brute force method. Although the computational expense of the algorithm is an issue, it is not the concern of this study. Later studies will address the computational requirements of the DMR beamformer, should it provide favorable acoustic performance. This study will determine whether favorable acoustic performance in a variety of noise environments can be obtained using the DMR beamformer.

Abraham and Owsley's study introduced a reduced-rank beamformer that had many qualities that made it favorable for this study. The DMR beamformer could easily be coded by modifying existing ABF algorithms. Also, the DMR beamformer should be easier to implement than other reduced-rank beamformers because the exact number of sources does not need to be known. However, the examples from Abraham and Owsley's study used only simulated data and only looked at a few of the issues associated with the DMR beamformer. This study expanded upon Abraham and Owsley's work and looked at some of the other issues involved with the DMR beamformer. These other issues include the perfor-

mance of the DMR beamformer using data from a real ocean environment, the sensitivity of the DMR beamformer to the parameters D, e, and σ^2, and the performance of the DMR beamformer using CSMs with reduced integration times.

3. ANALYSIS APPROACH

3.1 DESCRIPTION OF THE DATA SETS

Data from three experiments were chosen to evaluate the DMR beamformer's performance. All of the data sets were processed at the same frequency.

3.1.1 Deep Water Data Set (DWDS)

Data in the first experiment were acquired using a bottom-mounted horizontal line array (HLA) in a deep ocean environment. The water depth was about 1500 m. The array had eight hydrophones in a tapered design, and the length of the array was 2.4 wavelengths relative to the frequency processed.

The data were acquired from the array using a data acquisition system with a 12-bit A/D converter. One minute of data were recorded every 15 minutes. The data were low-pass filtered at 600 Hz and sampled at 2083.33 Hz. FFTs were calculated using a 2K transform length without any data overlap. Each set of the FFTs were used to calculate single sample CSMs that had 1 Hz bandwidths and 1 Hz center frequency spacings. After 61 single sample CSMs were calculated, they were averaged to obtain a single, 1 minute CSM, which was written to tape. Therefore the deep water data set CSMs contained 61 snapshots. Approximately 1 week of data was processed. Preliminary examination of DMR performance was done with these data.

3.1.2 Shallow Water Data Set #1 (SWDS1)

Data from the second experiment were obtained using a bottom-mounted horizontal line array in a shallow ocean environment. In this case, the water depth

was about 400 m. This array also had eight hydrophones in a tapered design and the length of the array was 3.4 wavelengths relative to the frequency processed.

The data were acquired from the array using an analog tape system and digitized at ARL:UT with a sampling rate of 800 Hz per channel. One minute of data were recorded every 10 minutes. The timeseries data were windowed using a Hanning window. The FFTs were calculated using a 4K transform length with 50% data overlap. The CSMs were calculated with various integration times and frequency bandwidths. For integration times shorter than 1 minute, only the first FFTs were used to calculate the CSMs and the rest of the FFTs for the minute were skipped. Table 3.1 shows the number of effective snapshots for the various integration times and frequency bandwidths of the first shallow water data set CSMs. One day of data was processed.

Table 3.1:
Number of effective snapshots for the SWDS1 CSMs.

Number of Time Averages	CSM Bandwidth		
	1 Hz	2 Hz	3 Hz
1	2.8	5.6	8.4
2	5.6	11.2	16.8
3	8.4	16.8	
4	11.2		
6		33.6	
7	19.6	39.2	
14	39.2	78.4	
21	58.8	117.6	

Note: shaded entries indicate that CSMs were not calculated for these combinations of time averages and bandwidths.

3.1.3 Shallow Water Data Set #2 (SWDS2)

Data from the third experiment were also obtained using a bottom-mounted horizontal line array in a shallow ocean strait. The water depth was about 475 m. The second shallow water data set array had 30 hydrophones. The complete 30 hydrophone array and subarrays with 8, 16, and 24 hydrophones were chosen to analyze. Table 3.2 shows the length of all the arrays used in this study. Table 3.2 shows that the 16, 24, and 30 hydrophone arrays are approximately the same length. Hence, the 24 and 30 hydrophone arrays are oversampled relative to the 16 hydrophone array.

Table 3.2:
Array lengths for the DWDS, SWDS1, and SWDS2.

Array	Array Length (wavelengths)
DWDS, 8 hydrophones	2.4
SWDS1, 8 hydrophones	3.4
SWDS2, 8 hydrophones	3.2
SWDS2, 16 hydrophones	8.3
SWDS2, 24 hydrophones	8.6
SWDS2, 30 hydrophones	8.6

Continuous data from the second shallow water data set were acquired from the array using a digital tape system with a sampling rate of approximately 1600 Hz per channel. The maximum FFT bandwidth was calculated to be approximately 0.4 Hz using the bandwidth constraint from Eq. (1.6). This bandwidth is smaller than the bandwidths from the other data sets because the SWDS2 arrays are longer than the arrays from the other data sets. The timeseries data were windowed using a Hanning window. The FFTs were calculated using a 4K transform

length with 50% data overlap. Using the bandwidth chosen above, the integration time and number of effective snapshots were calculated to keep the output power loss to $\leq$ 1 dB for each array. Table 3.3 shows the number of effective snapshots and integration time to maintain 1 dB of output power loss of the four array configurations. Four sets of CSMs were calculated with the integration times and number of effective snapshots from Table 3.3.

Table 3.3:
SWDS2 CSM parameters.

Number of Hydrophones	Number of Effective Snapshots	Integration Time (sec)
8	32.75	75
16	70.5	160
24	112.2	254
30	141.6	320

3.1.4 SWDS2 Array Configuration Beampatterns

Since four array configurations were used in processing the SWDS2, examining the array beampatterns is useful to assist in understanding how the arrays perform. In particular, the unshaded CBF beampatterns provide some insight as to how the ABF beampatterns will look when the noise is spatially white. Figure 3.1 shows the conventional positive endfire, or 90 degree beampatterns for the 8, 16, 24, and 30 hydrophone arrays. Beampatterns show how the beamformer operates on the signals in the environment described by the CSM. Signals in the direction where the beampattern is 1, or 0 dB, pass through the beamformer without attenuation. This direction is called the look direction, and the area surrounding the maximum at the look direction is referred to as the main lobe. The look direction for

the beampatterns in Fig. 3.1 is 90 degrees, or sinθ = 1.0. Signals or noise at directions away from the look direction are attenuated by the value of the beampattern in the corresponding directions. The region away from the main lobe is known as the sidelobe region. The sharp negative peaks are knows as nulls, due to the high attenuation in those directions.

Figure 3.1 shows the beampatterns for the conventional beamformer. Recall that the conventional beamformer does not use the information in the CSM about the interferers in the environment. Adaptive beamformers use the information in the CSM to create nulls in the direction of the interferers. Hence, the adaptive beamformer beampatterns will have the nulls in different places depending on the locations of the interferers in the data. However, the "undisturbed" adaptive beamformer beampattern will be the same as the conventional beampattern. Thus, plotting the conventional beampattern is useful to see some of the features of the ABF beampattern. Plotting the ABF beampattern would be impractical because at each time period, the ABF beampattern could be different due to the motion of the interfering sources.

The beampatterns are calculated by

$$M = w^H d \,. \tag{3.1}$$

The vectors d and w are the look direction steering vector and the signal direction vector, respectively, and are given by

$$\begin{aligned} w &= e^{-i2\pi f x \sin\phi/c}\,, \\ d &= e^{-i2\pi f x \sin\theta/c}\,, \end{aligned} \tag{3.2}$$

where f is the frequency, c is the speed of sound, θ is the look direction, and ϕ is angle at which the beamformer response is calculated.

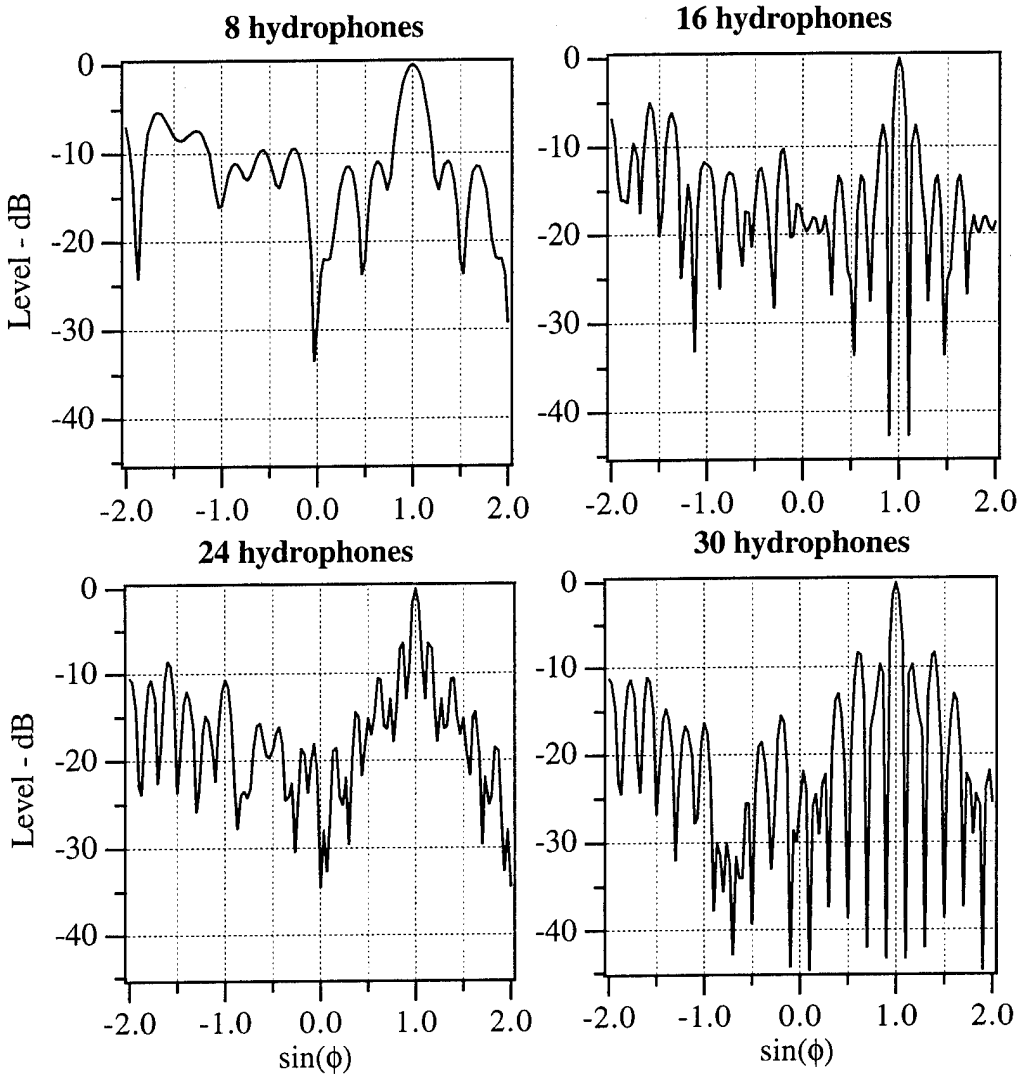

Figure 3.1 SWDS2 90 degree beampatterns for 8, 16, 24, and 30 hydrophones.

AS-96-4

The beampatterns are plotted for directions from $\sin\phi = -2.0$ to $\sin\phi = 2.0$. The beampatterns were calculated using values for $\sin\phi$, not ϕ. Therefore, values for $\sin\phi$ could be used to calculate the beampattern such that ϕ is outside the visible space. Only the area of the beampattern between $\sin\phi = -1.0$ and $\sin\phi = 1.0$ is in visible space, corresponding to $\phi = -90$ to 90 degrees. The beampatterns are

plotted outside the visible range for two reasons. First, these beampatterns allow more of the side lobe structure to be seen and analyzed. Second, when the look direction is at endfire ($\sin\phi = 1.0$), the side of the main lobe outside the visible range can be evaluated to determine if excessive squinting is occurring with adaptive beamformers.

Figure 3.2 shows an example beampattern that illustrates squinting and characteristics of beampatterns from adaptive beamformers. The look direction is approximately 25 degrees or $\sin\phi = 0.42$, and there is a loud interferer at approximately broadside (0 degrees) or $\sin\phi = 0.0$. The first thing to notice about Fig. 3.2 is that the adaptive beamformer creates a large null that is not present in the conventional beampattern in the direction of the interferer. Further, the sidelobe structure is completely different than the conventional beampattern. Also, the adaptive beampattern in Fig. 3.2 is for one time period, and the beampattern changes as the location of the interferers change. The second thing to notice about Fig. 3.2 is, when steered near the loud interferer, the adaptive beamformer response is still at 0 dB at the look direction. However, the null at approximately $\sin\phi = 0$ causes the beamformer response to be greater than 0 dB for directions between $\sin\phi = 0.42$ and 1.38. This effect, where the main lobe response is decreased on the side close to the interferer and the main lobe overshoots 0 dB on the other side, is known as squinting. The white noise gain constraint discussed in Section 2 limits the ability of the beamformer to squint to some extent.

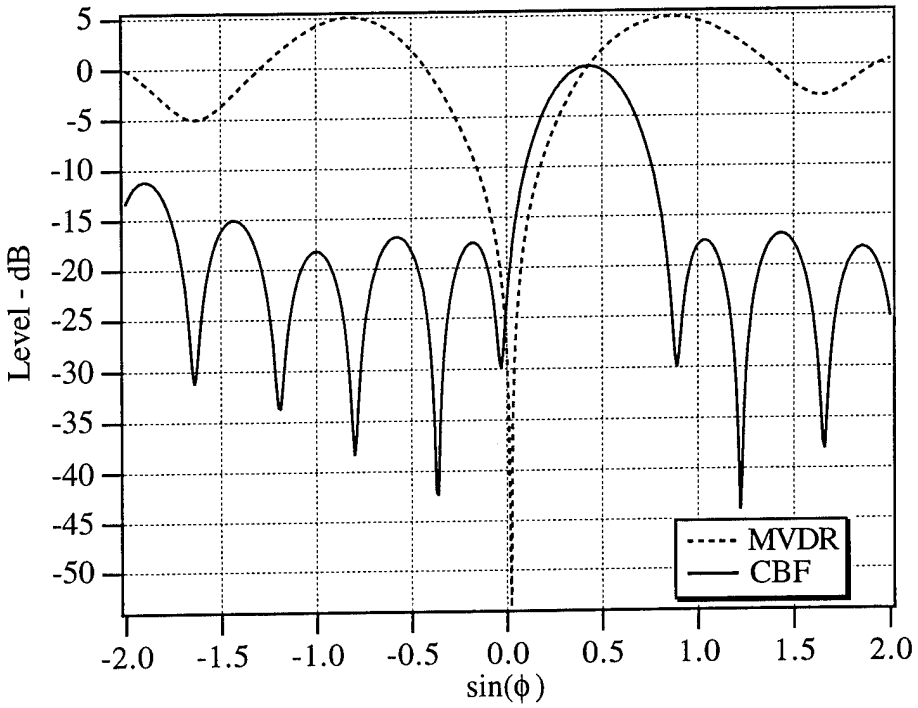

Figure 3.2 Example CBF and ABF beampatterns.

AS-96-5

Returning to Fig. 3.1, one important thing to notice about these plots is that the main lobe of the eight hydrophone array is twice as wide as the main lobe of the other arrays. This occurs because the width of the main lobe is inversely proportional to the length of the array, and the eight hydrophone array is half as long as the other arrays.

The main lobe width of the beampatterns also affects the number of beams, or look directions, required to cover all of the visible space. The attenuation level where two adjacent look direction main lobes cross is referred to as the scalloping loss. The scalloping loss is a function of the main lobe width and the number of beams. The scalloping loss increases as the frequency increases for the current beamforming scheme. If the scalloping loss is too large, a desired signal can be

missed if it appears between beams. The scalloping loss was calculated for each array, and a number of look directions was chosen so that the scalloping loss was less than 1 dB. Twenty five look directions were chosen for the 8 hydrophone array, and 61 look directions were chosen for the 16, 24, and 30 hydrophone arrays. Since the 16, 24, and 30 hydrophone arrays are the same length, their scalloping losses and number of look directions are the same.

These plots also show why arrays with more hydrophones can perform better than arrays with fewer hydrophones. The beampatterns from well designed arrays with more hydrophones have lower sidelobes than beampatterns from arrays with fewer hydrophones. For example, the maximum 16 hydrophone beampattern sidelobe is approximately –5 dB, but the maximum 30 hydrophone beampattern sidelobe is approximately –9 dB. Therefore, for arrays with more hydrophones, noise away from the look direction can be attenuated further. Thus, the beam noise in the quiet directions between interferers will be lower, providing better beamformer performance. Also, adaptive beamformers using more hydrophones can perform better than adaptive beamformers using fewer hydrophones because beamformers using more hydrophones have more degrees of freedom to place more nulls in the beampattern to null the interferers.

3.2 ANALYSIS APPROACH AND METHODOLOGY

The deep water and the shallow water data sets were processed on the ARL:UT Alliant and Sun SPARCcenter 2000 computers. First, the data sets were processed using unshaded conventional beamforming (CBF). Following the CBF processing, the data sets were processed with ARL:UT's MVDR and WNGC ABF. These results provide a baseline of results to compare to the DMR performance.

Once the baseline processing was completed, the data sets were screened by calculating the eigenvalues of the CSMs. The number of loud interferers in the environment could be determined from the eigenvalues of the CSM, and then D could be chosen so that all of the loud interferers would be included in the CSM estimate. Next, DMR performance sensitivity to variations in e and σ^2 was examined for the deep water data set and compared to the baseline results. Initial values of e and σ^2 were chosen that allowed the DMR beamformer performance to emulate the WNGC beamformer performance. Then, DMR performance was examined, with the selected values of e and σ^2, using CSMs from the two shallow water data sets.

4. DEEP WATER DATA SET RESULTS

As discussed in Section 3, the initial studies using DMR were performed with the deep water data (DWDS) set. In this case CSMs had been calculated with a fixed integration time. Hence, only limited performance assessments could be made without reprocessing. However, the data provide a basis for determining some of the DMR parameters that were used in the shallow water data set analysis.

Recall that one of the objectives of this study is to determine if the DMR beamformer can provide performance equivalent to the WNGC beamformer but use shorter CSM integration times than required by the WNGC beamformer. The WNGC is used as the standard because it has been shown to provide robust gain against interferers for a wide variety of noise fields. Thus, the DWDS will be used to determine the parameter values that allow the DMR beamformer to emulate the WNGC beamformer. Then these parameter values will be tested with the two shallow water data sets. If the DMR beamformer performance is close to the WNGC beamformer for the other noise environments, then the DMR parameters are satisfactory. It is possible that other settings for the DMR parameters improve the DMR performance. However, this study is interested in determining whether favorable acoustic performance is feasible using the DMR beamformer.

4.1 DWDS BEAM NOISE

Figure 4.1 shows the beam noise for unshaded CBF, and Fig. 4.2 shows the beam noise for MVDR and WNGC ABF. In both figures, a seismic profiler that turns on and off at semi-regular intervals is visible at $\sin\theta = 0.8$. The profiler is

much louder, by at least 10 dB, than any other noise source. This will influence the number of large eigenvalues in the CSM when the profiler is on.

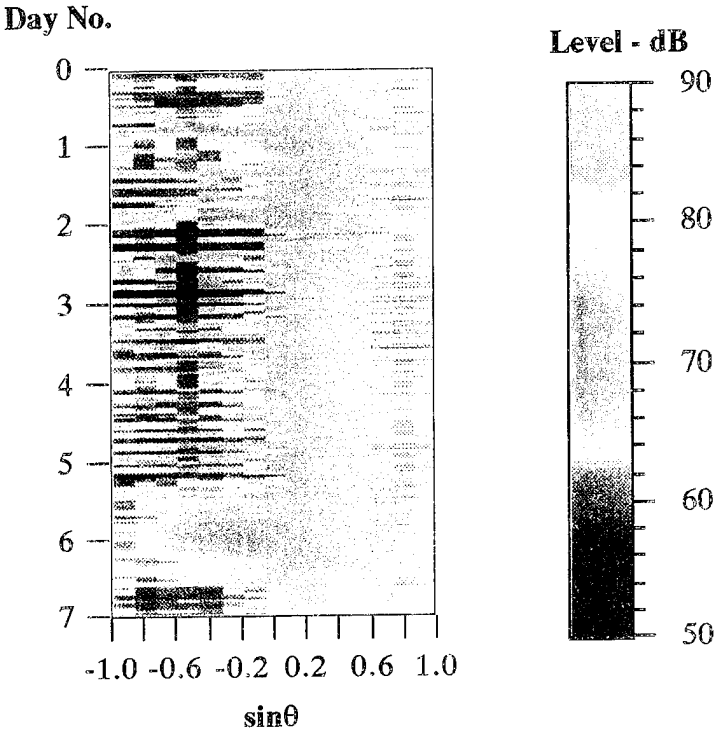

Figure 4.1 DWDS CBF beam noise.

AS-96-6

Comparing the CBF plots (Fig. 4.1) with the ABF plots (Fig. 4.2) shows that the ABF noise levels are much quieter than the CBF levels between $\sin\theta = -1.0$ and $\sin\theta = 0.0$. This is because the adaptive beamformer can null out the loud source (at $\sin\theta = 0.8$) when the beamformer is steered in these quiet directions. Also, the WNGC ABF levels are close to the CBF levels in the direction of the interfering source, indicating that the white noise gain constraint is providing sufficient robustness to restrict losses due to mismatch.

The MVDR levels (Fig. 4.2), however, are lower than the WNGC ABF levels in the direction of the loud source (at $\sin\theta = 0.8$). This is due to the lack of the

white noise gain constraint for the MVDR case. Since the loud source is not exactly in one of the look directions, the MVDR beamformer squints away from the loud source, reducing its received level. Also, multipath and other sources of mismatch contribute to the reduction in the received level. On the other hand, there is in not much difference between the quiet regions in the MVDR and the WNGC ABF plots, indicating that there is very little penalty for setting the white noise gain constraint to –3 dB.

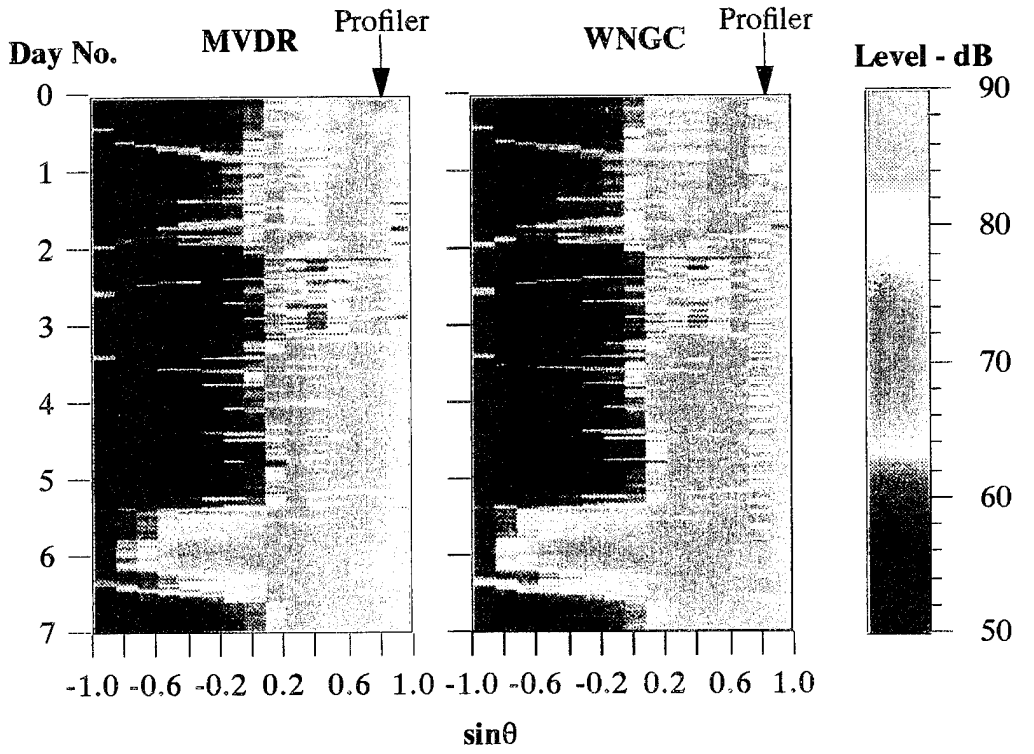

Figure 4.2 DWDS WNGC ABF and MVDR beam noise.

AS-96-7

4.2 DWDS EIGENVALUES

Figure 4.3 shows the eigenvalues of the DWDS CSM. All the eigenvalues are scaled by the largest eigenvalue so that the largest eigenvalue is always one. In these plots, the number of large eigenvalues varies from one large eigenvalue to three or four large eigenvalues for most time periods. This switching corresponds to the profiler seen in the beam noise plots. This is clear in Fig. 4.4, which shows the eigenvalues and beam noise together.

When the profiler is on, it dominates the noise field and is associated with the single eigenvalue that is significantly larger (10 dB) than the other eigenvalues (see point A). When the profiler is off, there are several significant noise sources, and consequently there are several eigenvalues of the same order of magnitude (see point B). This is consistent with the assumption that the largest eigenvalues of the CSM are associated with loudest noise sources in the environment described by the CSM.

For most time periods, the first four eigenvalues contain the top 15–20 dB of the noise field. For this reason, a CSM based on the first four eigenvalues would contain much of the information about the spatial properties of the noise field.

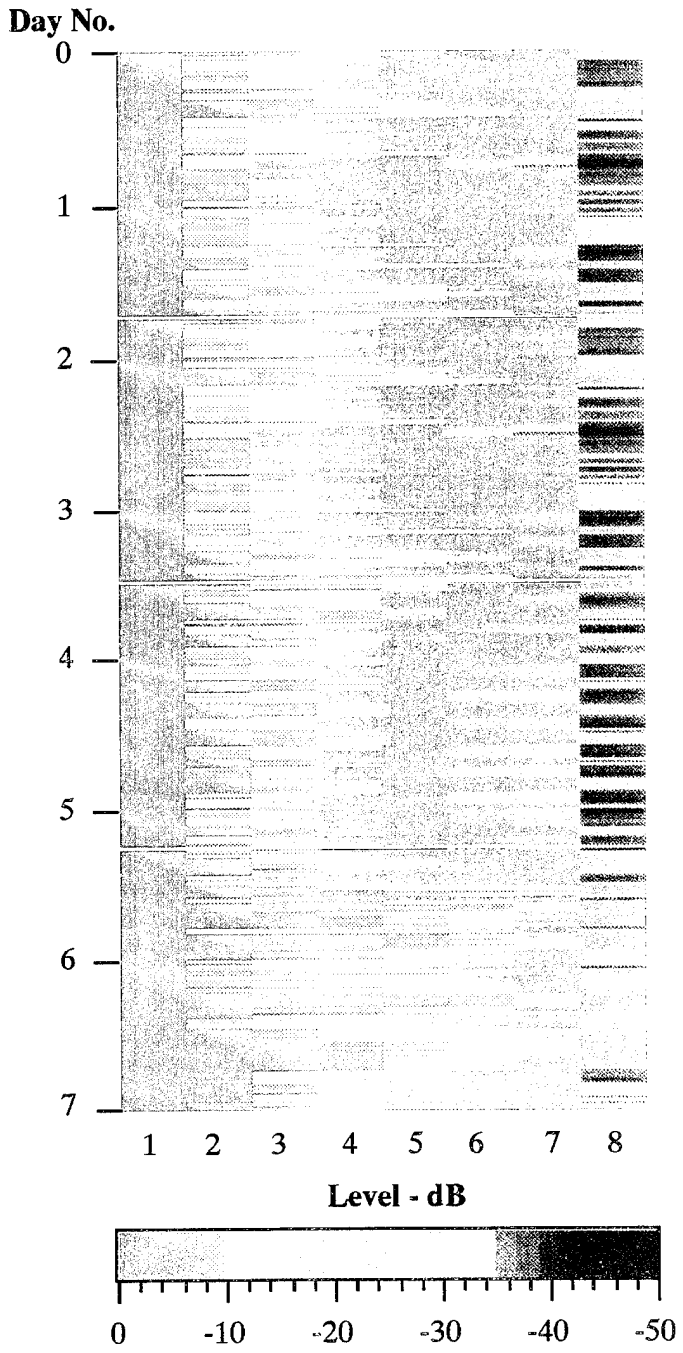

Figure 4.3 DWDS eigenvalues in decibels relative to the largest eigenvalue.

AS-96-8

This page intentionally left blank.

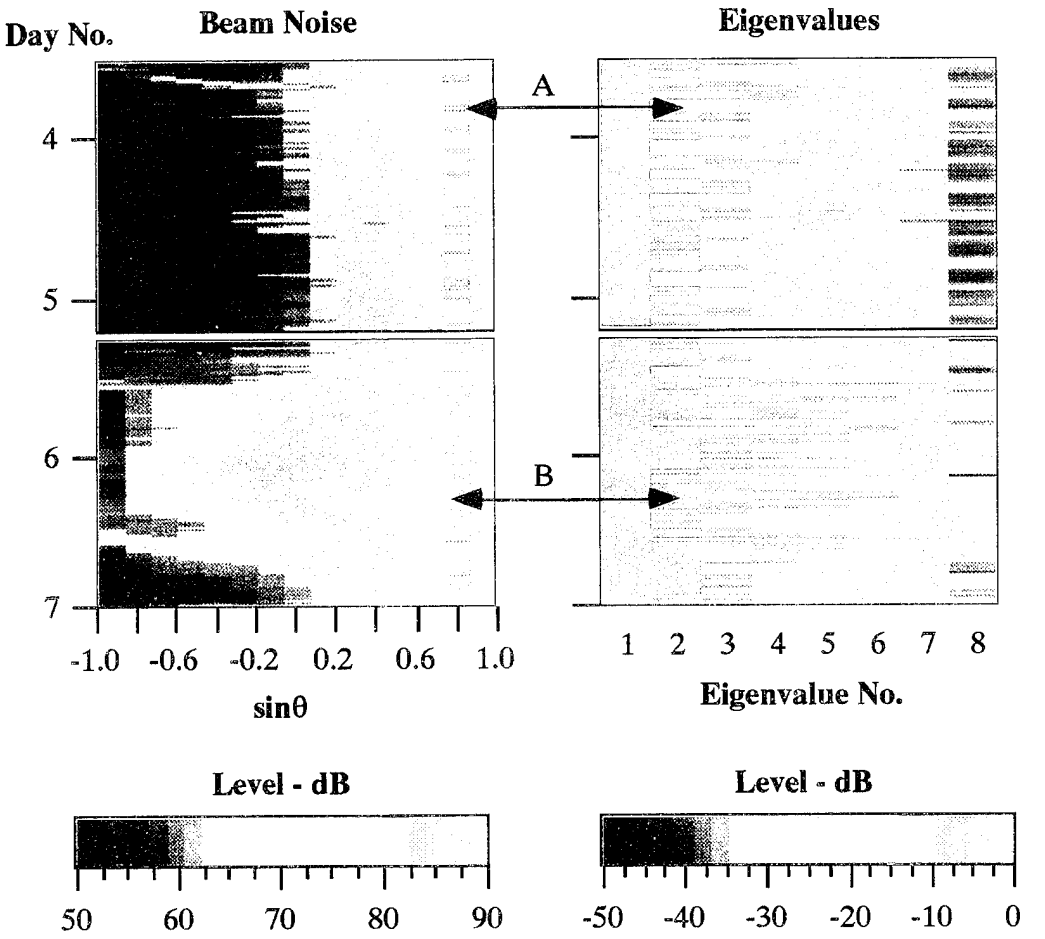

Figure 4.4 DWDS beam noise and eigenvalues.

AS-96-9

4.3 DWDS WHITE NOISE GAIN

Recall from Section 1 that the white noise gain is a measure of the robustness of a beamformer. Thus, in order to determine if the DMR beamformer can provide robust performance, the white noise gain values from the DMR beamformer must be evaluated. The WNGC beamformer is known to be robust to mismatch errors; therefore the white noise gain values of the DMR beamformer will be compared to the white noise gain values of the WNGC beamformer. The white

noise gain constraint is set 3 dB below 10log$N$, or at 6 dB for the WNGC beamformer.

Figure 4.5 shows the white noise gain percentiles for MVDR and WNGC ABF. Figure 4.5 illustrates that the white noise gain values for the MVDR case can be very small (-20 dB), showing this beamformer is very sensitive to mismatch. Many of the low values are associated with times (and look directions) when the beamformer is steered near the loud interferer as seen from Fig. 4.2. When the white noise gain constraint is applied, the white noise gain never falls below 6 dB and hence provides a guard against mismatch.

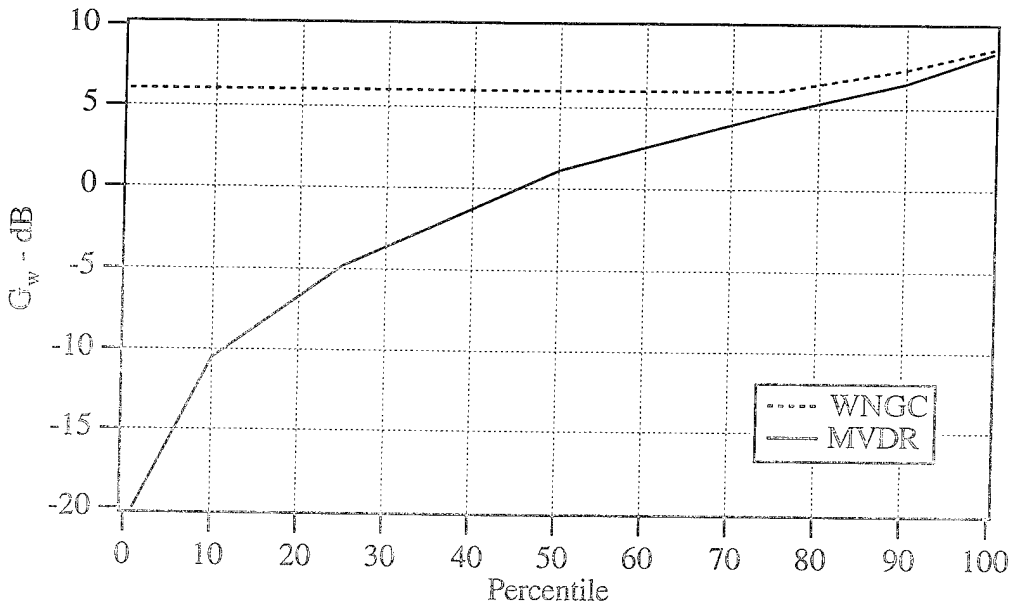

Figure 4.5 DWDS MVDR and WNGC white noise gain percentiles.

AS-96-10

4.4 DETERMINATION OF APPROPRIATE σ^2 AND e VALUES

As discussed earlier in Section 2.2, values of e and σ^2 must be chosen. Remember from Section 2.2 that e is used as an "enhancement factor" for the eigenvalues and thus controls the amount of information in the CSM that is used in calculating the weights. σ^2 governs the amount of uncorrelated noise added to the diagonal of the CSM. This noise keeps the CSM nonsingular and forces all the signals in the environment described by the reduced rank CSM other than the D dominant sources to be uncorrelated noise.

In this study, the performance of the DMR beamformer is being compared directly with the fully adaptive beamformer with a white noise gain constraint set to 3 dB below 10log$N$. Recall that Fig. 4.2 showed that this level of the constraint provides reasonable robustness against mismatch, while not penalizing the quiet sector performance. The beam noise and white noise gain values of a beamformer were used to determine values of e and σ^2 so that the DMR beam noise and white noise gain values emulated the WNGC beamformer beam noise and white noise gain values as closely as possible. This was accomplished by examining the sensitivity of the DMR beamformer to e and σ^2 by processing the DMR beamformer on a small part of the DWDS. These results are discussed in Sections 4.4.1 and 4.4.2.

4.4.1 DMR Sensitivity to σ^2

To begin the sensitivity studies, e was set to 1.0 and the DMR beamformer was run for several different values of σ^2 for a small amount of the DWDS data. In their work, Abraham and Owsley[3] used e values of 1 and 10 because they wanted a MUSIC like angular response spectrum with sharper lobes in the look direction at the expense of the nulls in the direction of the interferers. This study, on the other hand, was more interested in nulls for the interferers than in extremely sharp look

direction lobes; therefore, e values from 0 to 1 were used. For this initial study, e was set to 1.0 because when e is 1.0 and D is set to the number of hydrophones in the array so that all of the eigenvalues and eigenvectors are used to approximate the CSM, the CSM is reconstructed completely and the DMR beamformer is equivalent to the MVDR beamformer.

Figure 4.6 shows the beam noise for 14 sequences, or 3 hours of data, where the value of σ^2 has been varied from 0.005 to 0.5. Figure 4.6 also shows the WNGC ABF result for comparison. It is clear that the beam noise levels in the quiet direction ($1.0 \leq \sin\theta \leq 0.0$) are dependent on the σ^2 selection. Larger values of σ^2 show a penalty of increased beam noise. As σ^2 decreases, the DMR beam noise looks most like the WNGC ABF beam noise. At $\sigma^2 = 0.005$, the amount added to the CSM diagonal is 23 dB down from the largest eigenvalue's contribution. Since the noise data of interest (in terms of forming the weights) is contained in the top 10–20 dB, having a σ^2 of 0.005 provides a reasonable noise floor.

Figure 4.7 shows the white noise gain percentiles for the same cases. It is clear that the white noise gain values are not affected in any organized manner by the choice of σ^2. Thus the beam noise values were used to determine the value of σ^2 for the DMR beamformer, and σ^2 was chosen to be 0.005 because this value provides a reasonable noise floor, and with this value the DMR beam noise looks most like the WNGC ABF beam noise. Next, σ^2 was set to 0.005 and the DMR beamformer was run for several different values of e.

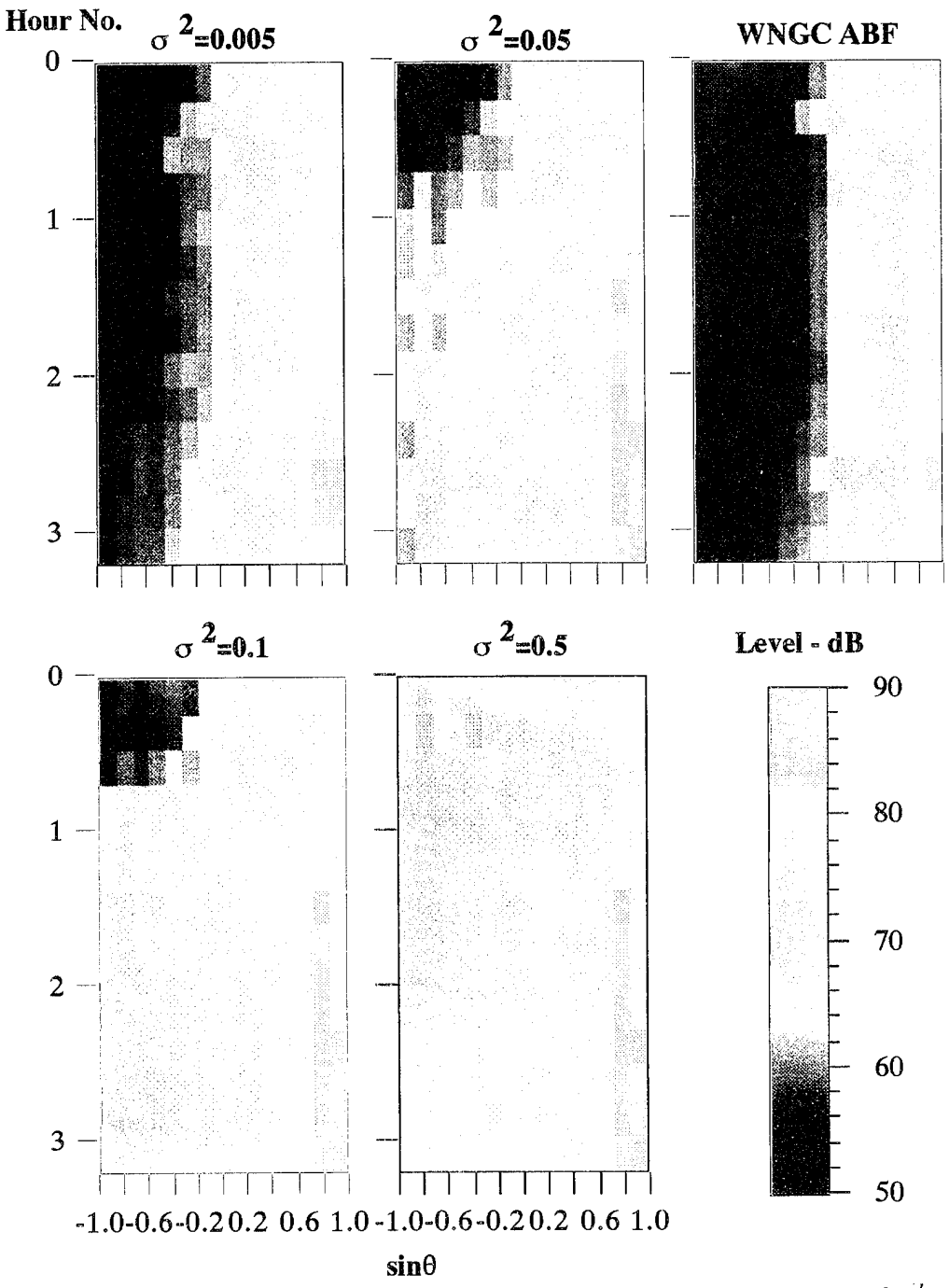

Figure 4.6 DWDS DMR beam noise with e = 1.0 and varying values of σ^2.

AS-96-11

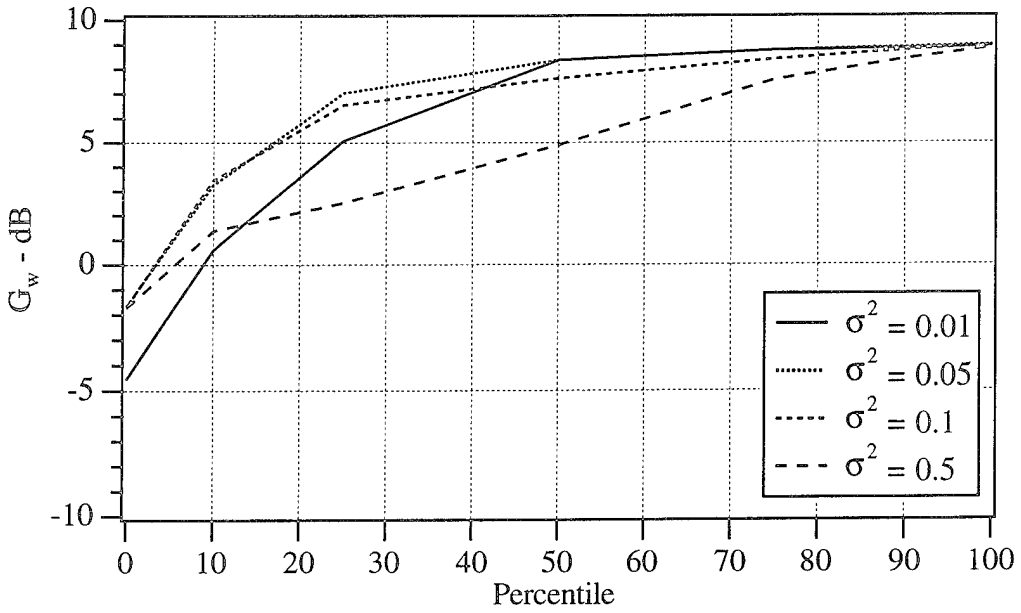

Figure 4.7 DWDS DMR white noise gain percentiles for e = 1.0 and varying values of σ^2.

AS-96-12

4.4.2 DMR Sensitivity to e

Figure 4.8 shows the beam noise for the same 3 hours of data, but this time, the value of σ^2 has been set to 0.005 and the value of e has been varied from 0.3 to 1.0. It is clear that there is very little difference between the beam noise plots for different values of e; hence the beam noise levels do not depend greatly on the selection of e. Thus the white noise gain statistics were used to determine the value of e for the DMR beamformer.

Figure 4.9 shows the white noise gain results for the same cases. Unlike the earlier plots with different values of σ^2, the white noise gain plots are affected by the choice of e. Larger values of e show a penalty of decreased white noise gains, which means the beamformer is more sensitive to mismatch. As e decreases, the DMR white noise gain statistics look most like the WNGC ABF white noise gain statistics.

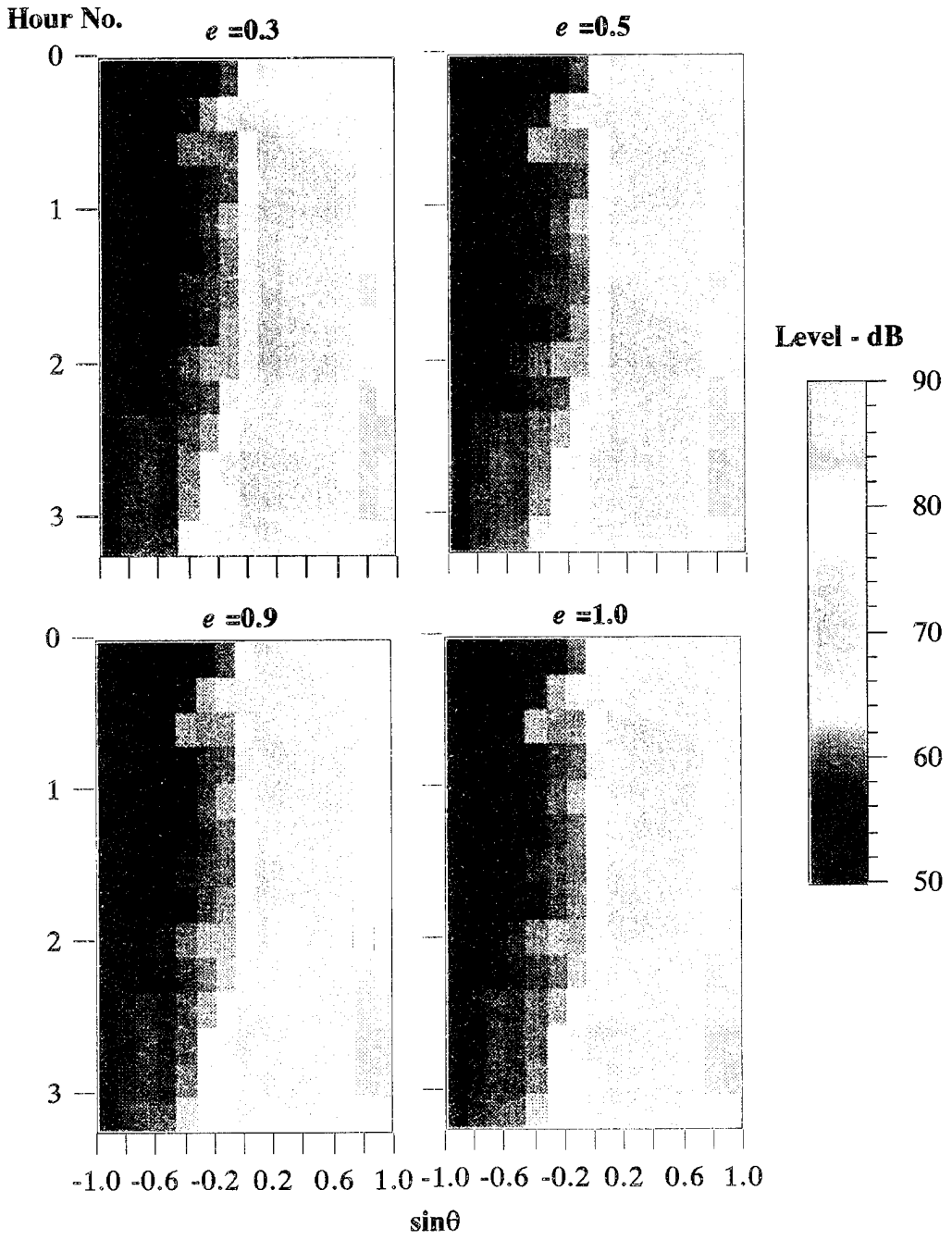

Figure 4.8 DWDS beam noise with $\sigma^2 = 0.005$ and varying values of e.

AS-96-13

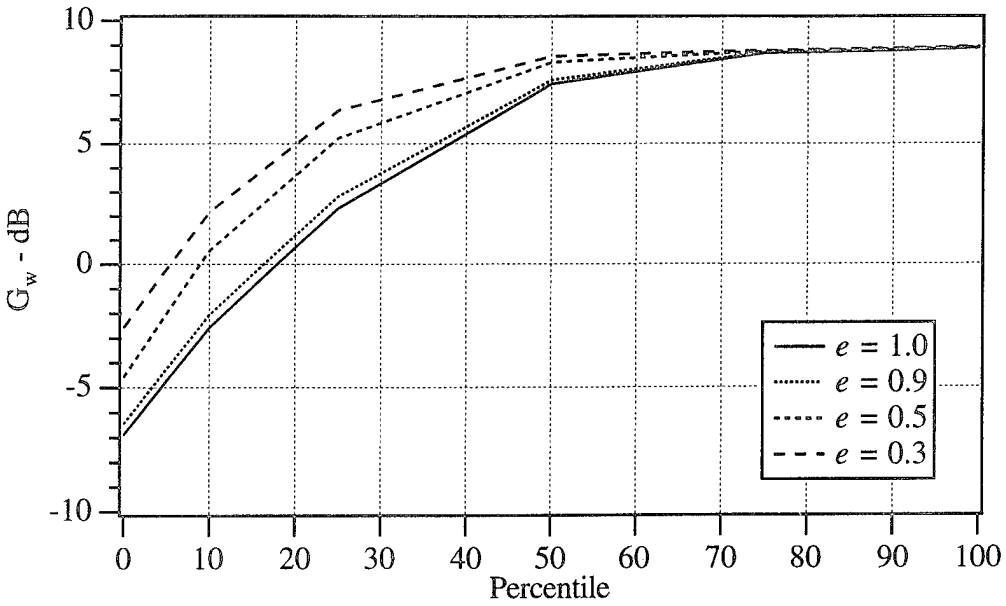

Figure 4.9 DWDS DMR white noise gain for $\sigma^2 = 0.005$ and varying values of e.
AS-96-14

The $e = 0.5$ value was chosen because the 25% point is approximately 5 dB and the 10% point is above 0 dB. This means that almost 75% of the white noise gains are above 5 dB and 90% of the white noise gains are above 0 dB. This is to be compared with the WNGC ABF statistics where all of the white noise gains are constrained above 6 dB. Thus, almost 75% of the DMR white noise gain values are equivalent to the WNGC white noise gain values. Also, most of the low white noise gain values occur when the beamformer is pointed at the profiler, where there is less concern about signal suppression.

The final values for e and σ^2 using the DWDS are 0.5 and 0.005, respectively. These values allow the DMR beamformer to show similar gains in the quiet directions and similar levels of robustness relative to the WNGC beamformer. These values were chosen by processing the DMR beamformer with a constant e and varying values of σ^2 to choose a value for σ^2. Then, the data were processed with the DMR beamformer using the chosen value of σ^2 and varying values of e to choose a value for e. This method is justified because e and σ^2 have a linear rela-

tionship with respect to the reduced-rank CSM estimate from Eq. (2.9). Thus, each variable should affect the reduced-rank CSM estimate independently. These settings were based on a small fraction of the DWDS data. Given these settings, it is important to determine how well the DMR beamformer performs for the entire data set.

4.5 DWDS DMR BEAM NOISE

After values for e and σ^2 were chosen, the DMR beamformer performance was examined with these values. Figure 4.10 shows the beam noise from the DMR beamformer for the whole week of data with $D = 4$, $e = 0.5$, and $\sigma^2 = 0.005$. Recall that the goal of the DWDS calculations was to determine the values of e and σ^2 that caused the DMR beamformer to perform most like the WNGC beamformer. Comparing the DMR beam noise with the CBF and ABF beam noise from Figs. 4.1 and 4.2 shows that the DMR noise levels are very similar to the WNGC ABF levels. Between $\sin\theta = 0.0$ and $\sin\theta = 1.0$, the DMR beam noise is almost identical to the WNGC ABF beam noise. Also, the DMR beam noise levels are close to the CBF beam noise levels in the direction of the loud interferer at $\sin\theta = 0.8$. Thus, the DMR beamformer is providing sufficient robustness to restrict the losses due to mismatch.

Like the WNGC ABF case, the DMR beam noise is much quieter than the CBF beam noise between $\sin\theta = -1.0$ and $\sin\theta = 0.0$ because the DMR beamformer nulls out the loud source at $\sin\theta = 0.8$ when the beamformer is steered away from this loud source. The DMR beam noise is close to the WNGC ABF beam noise, but it is slightly louder than the WNGC ABF in the quietest areas.

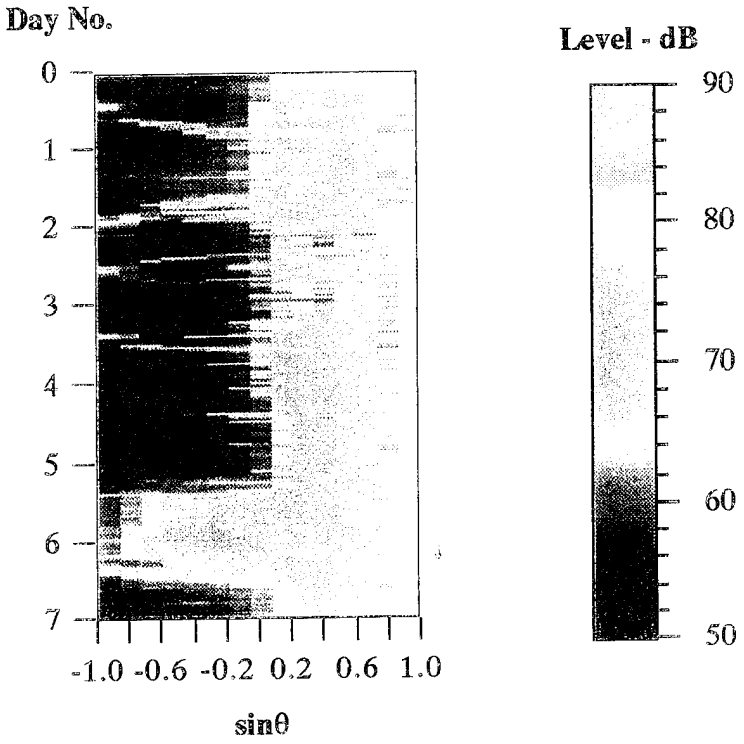

Figure 4.10 DWDS DMR beam noise.

AS-96-15

Further examination of the difference between the DMR and the WNGC ABF beam noise is aided by Fig. 4.11, which shows the DMR beam noise levels relative to the WNGC ABF beam noise levels. Most of the DMR beam noise levels are within 3 dB of the WNGC ABF beam noise levels. However, the DMR beam noise levels are 6 dB louder than the WNGC ABF beam noise levels during days 5 and 6 for most of the look directions. In fact, the DMR noise is louder than the CBF noise at $\sin\theta = 0.2$. This is during a period when the CBF and ABF noise are essentially the same and no dominant source appears in the noise field. It is likely that some feature of the eigenvalues and eigenvectors during this period is causing

this result. Additional work at a later date is warranted to examine the reason for this result.

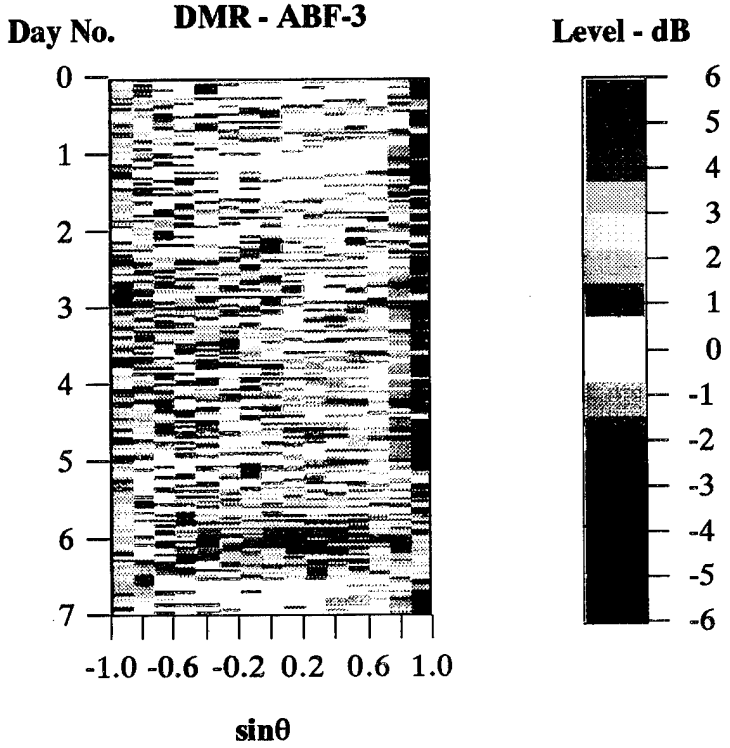

Figure 4.11 Difference of DWDS DMR and WNGC ABF beam noise.
AS-96-16

4.6 DWDS SUMMARY

The DWDS analysis shows that the DMR beamformer appears to work as expected. The DMR beamformer has more parameters to adjust than the standard adaptive beamformer. The number of eigenvalues, *D,* must be chosen as well as the scalar enhancement factor, *e,* and the noise factor, σ^2; however, $e = 0.5$ and $\sigma^2 = 0.005$ appear to work well on the DWDS data. With these values for e and σ^2, the DMR beamformer suitably emulates the WNGC beamformer such that most of

the DMR beam noise levels are within 3 dB of the WNGC ABF beam noise levels. There is a period in which no dominant source appears in the noise field and the DMR beam noise levels are louder than the CBF noise levels. Additional work might be warranted to examine the reason for this result. Otherwise, the parameters found for this application of DMR seem reasonable. The DWDS analysis indicates that favorable acoustic performance is possible using the DMR beamformer, provided the DMR settings are not overly sensitive to the noise environment. Sections 5 and 6 will describe tests of these settings with two different noise environments.

5. SHALLOW WATER DATA SET #1 RESULTS

Only CSMs with 1 minute integration times were available from the deep water data set. Therefore, the initial studies using DMR were performed on the deep water data set, and the initial values for D, σ^2, and e were chosen. Following this work, additional processing was performed on a second data set that had different CSM integration times. The first shallow water data set (SWDS1) was used to determine if the DMR beamformer could overcome the bias errors associated with standard adaptive beamformers with the reduced CSM integration times.

5.1 SWDS1 BEAM NOISE

Figures 5.1 and 5.2 show the WNGC ABF and MVDR beam noise for CSMs that had 2.8, 5.6, 19.6, and 58.8 snapshots (corresponding to 2.5, 5.1, 17.9, and 53.8 s integration time). From these plots, it is clear that the beam noise for the SWDS1 decreases as the CSM integration time decreases. Section 1 explains that the accuracy of the CSM is directly proportional to the integration time of the CSM. When the integration time is small, the CSM estimate is inaccurate and the standard adaptive beamformer will give biased results. Hence, the beam noise results for the 2.8 and 5.6 snapshot CSMs for WNGC ABF and MVDR are biased low. The beam noise bias also affects the signal on boresight as well. It is important to note that work at ARL:UT has shown that the SNR of signals on boresight decreases as the beam noise decreases. Thus the biased noise estimates do not indicate improved performance. The eigenvalues of the CSMs for this data set give some insight about why the beam noise is biased.

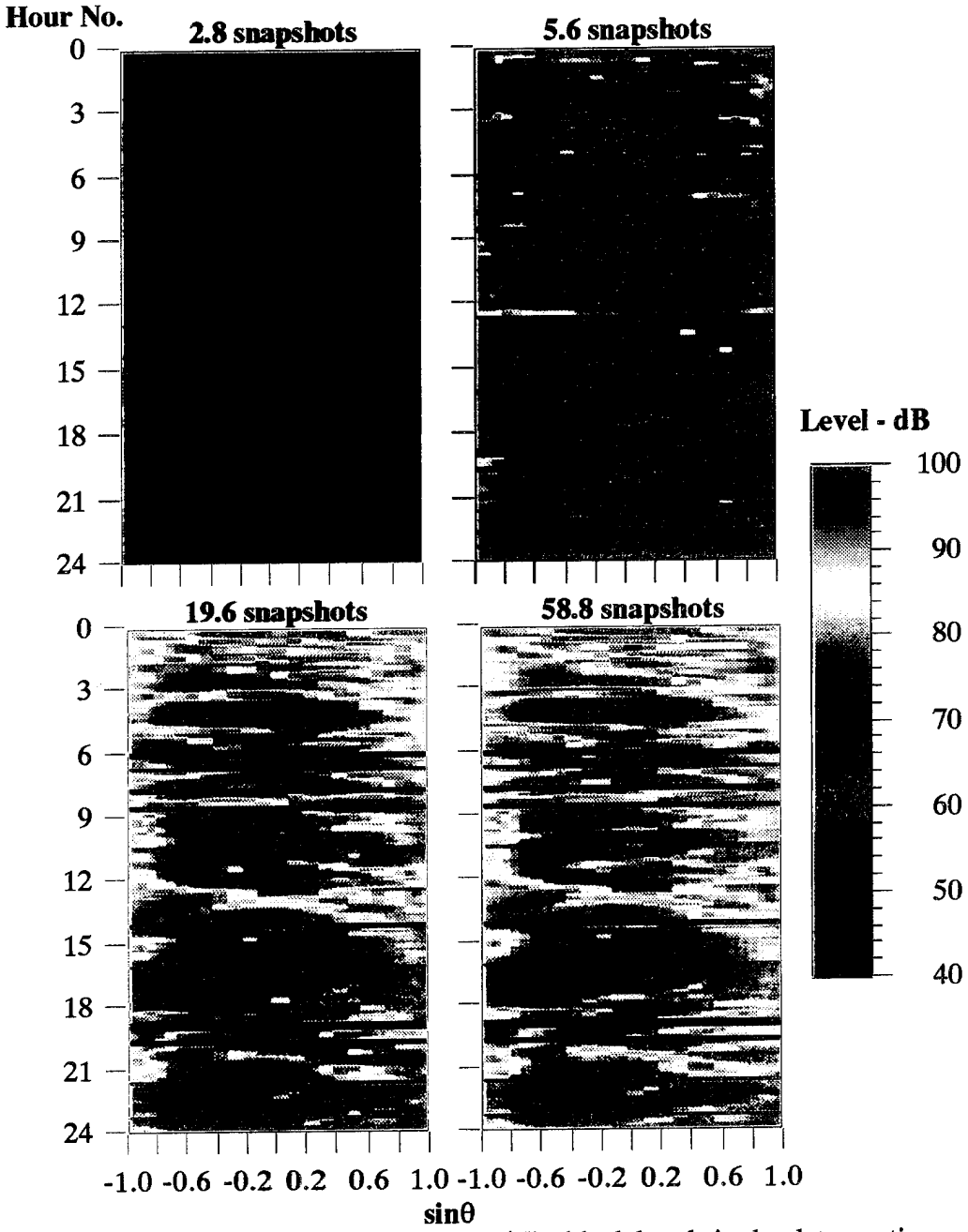

Figure 5.1 SWDS1 MVDR beam noise. (The black bands in the data are times when the analog tape data were of insufficient quality to create time-aligned FFTs. The black bands are not seen in the 2.8 snapshot plot because the beam noise is so low that if it were plotted to show the black bands, the purple regions would be black as well.)

AS-96-17

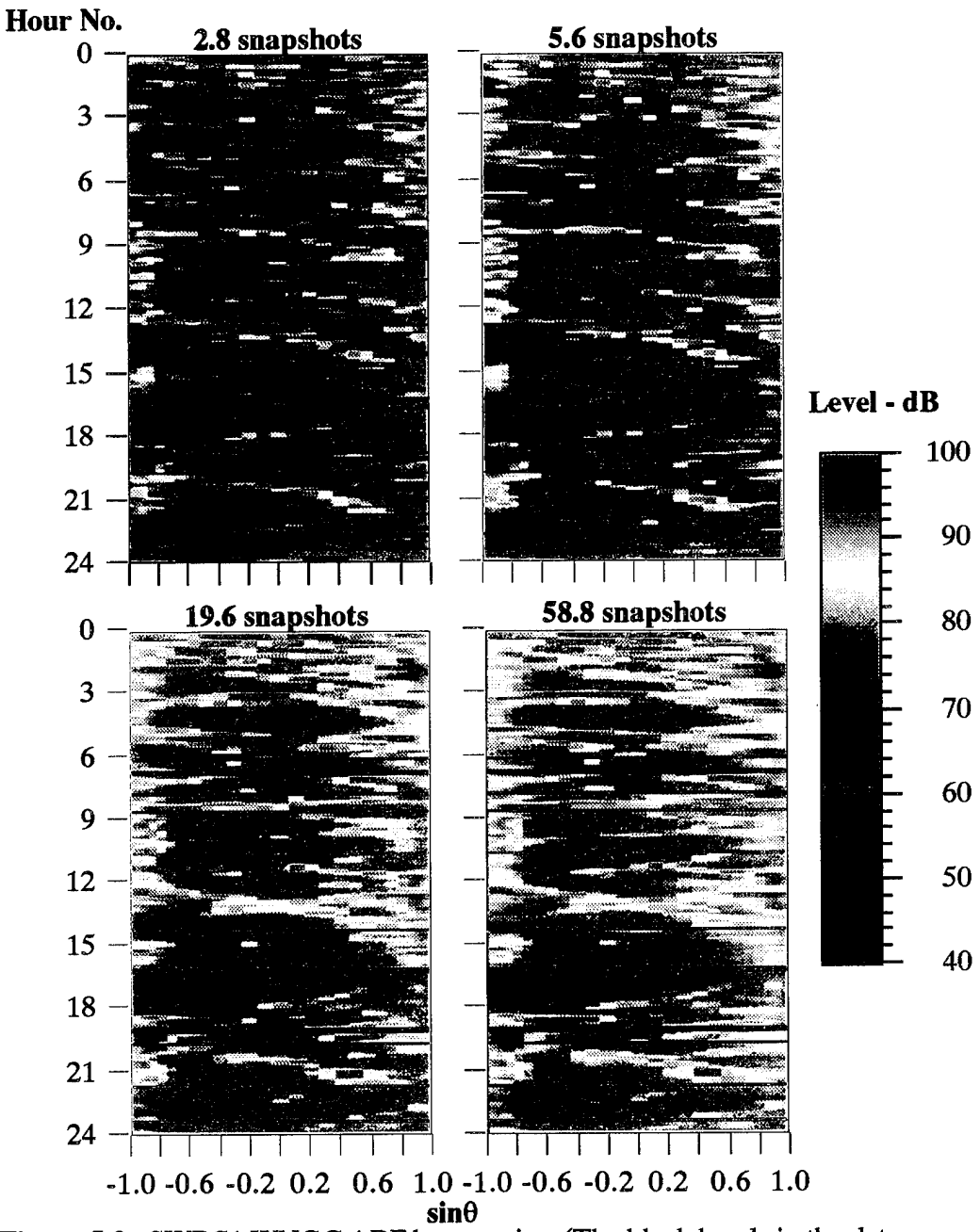

Figure 5.2 SWDS1 WNGC ABF beam noise. (The black bands in the data are times when the analog tape data were of insufficient quality to create time-aligned FFTs. The black bands are not seen in the 2.8 snapshot plot because the beam noise is so low that if it were plotted to show the black bands, the purple regions would be black as well.)

AS-96-18

5.2 SWDS1 EIGENVALUES

Figure 5.3 shows the eigenvalues of the CSM. Again, all the eigenvalues are scaled so that the largest eigenvalue is always one. Figure 5.3 shows that the last three eigenvalues of the CSMs made with 2.8 snapshots are extremely small. When the standard adaptive beamformer used these eigenvalues, it gave the biased beam noise results seen in Figs. 5.1 and 5.2. This is because the weights are a function of the inverse of the CSM, and the inverse of the CSM is calculated by

$$R^{-1} = \frac{1}{\lambda} UU^H, \tag{5.1}$$

where λ are the eigenvalues and U are the eigenvectors of the CSM.

If one or more of the eigenvalues are very small, they will dominate the solution, and if the eigenvalues are small and wrong, the solution will also be wrong. However, the DMR beamformer uses only the D largest eigenvalues, so if D is chosen to be less than five, the DMR beamformer should give better results than the standard adaptive beamformer.

For this study, D was also chosen to be four because the first four eigenvalues contain the top 15 dB of the noise field. Then the DMR beamformer was run with the values of σ^2 and e that were found to work best with the deep water data set, and the DMR beam noise was examined.

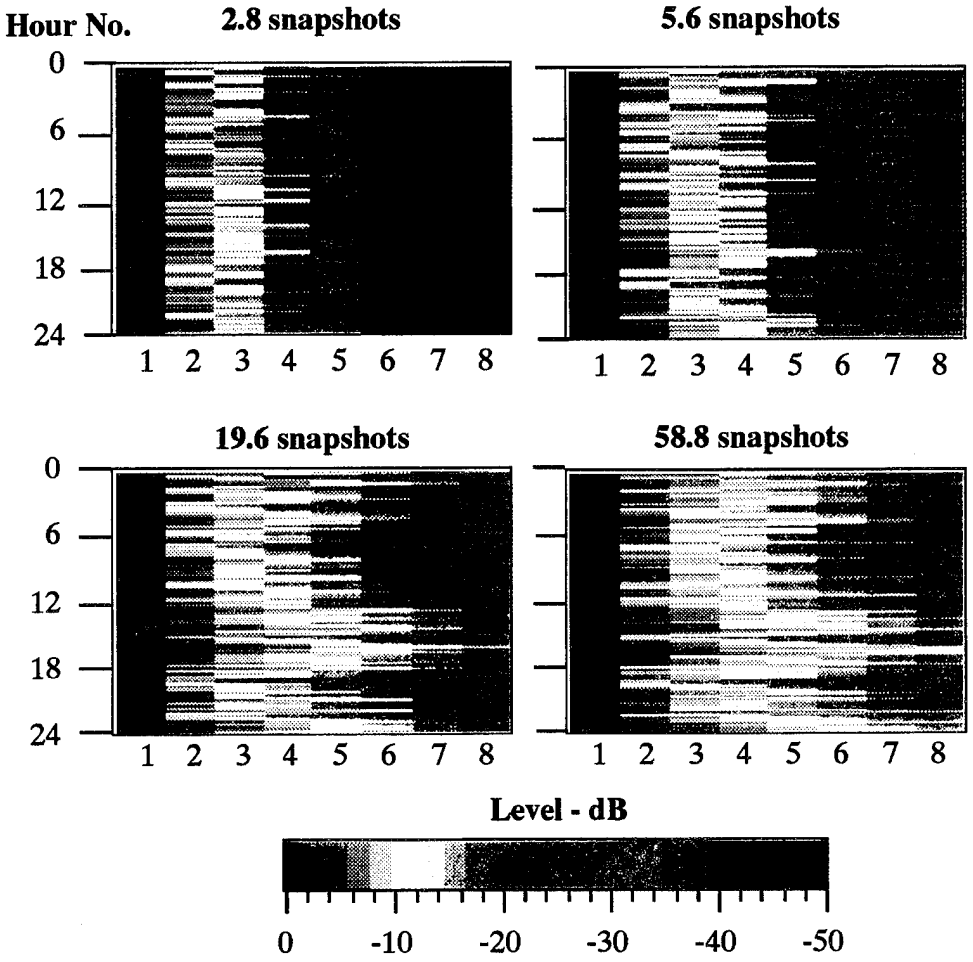

Figure 5.3 SWDS1 eigenvalues.

AS-96-19

5.3 SWDS1 DMR BEAM NOISE

Figures 5.4 and 5.5 show the beam noise plots for the DMR beamformer with $D = 4$, $\sigma^2 = 0.005$, $e = 0.5$ and with $D = 4$, $\sigma^2 = 0.005$, $e = 1.0$. Compared to Figs. 5.1 and 5.2, the beam noise for the CSMs with the small integration times is more realistic when using the DMR beamformer. Hence, the beam noise bias is reduced with the DMR beamformer. Further, the beamformer performs well with

the parameter values derived from the DWDS, indicating that the DMR beamformer's performance in different noise environments is not overly sensitive to the σ^2 and e settings.

Examining these four figures in further detail shows the DMR beamformer beam noise based on the 2.8 and 5.6 snapshot CSMs is much closer to the 19.6 and 58.8 snapshot CSM beam noise derived using WNGC ABF. For WNGC ABF, the 2.8 snapshot CSM beam noise is $30-40$ dB quieter and the 5.6 snapshot CSM beam noise is 10–20 dB quieter than the 19.6 and 58.8 snapshot CSM beam noise. In contrast, the DMR beam noise using the 5.6 snapshot CSMs is only 4 dB quieter than the WNGC 19.6 snapshot CSM beam noise.

Grant et al.[1] found that for the SWDS1, the best WNGC ABF results were obtained using a CSM estimate with approximately 19.6 snapshots. That is, with 19.6 snapshots, the integration time is sufficient to limit the noise bias to acceptable levels, and the integration time is sufficiently short to capture the dynamics of the noise. The DMR beamformer beam noise from the 5.6 snapshot CSM is close to the WNGC beamformer beam noise from the 19.6 snapshot CSM. Therefore, for this data set, the DMR beamformer could be used with the 5.6 snapshot CSM, lowering the required integration time by a factor of 3.5. Given that a longer integration time can be used for the noise environment, an array with more hydrophones could be used, with the number of eigenvalues set appropriately for 19.6 snapshots. Thus additional gain might be attainable without increasing the CSM integration time. This is addressed further in Section 6.

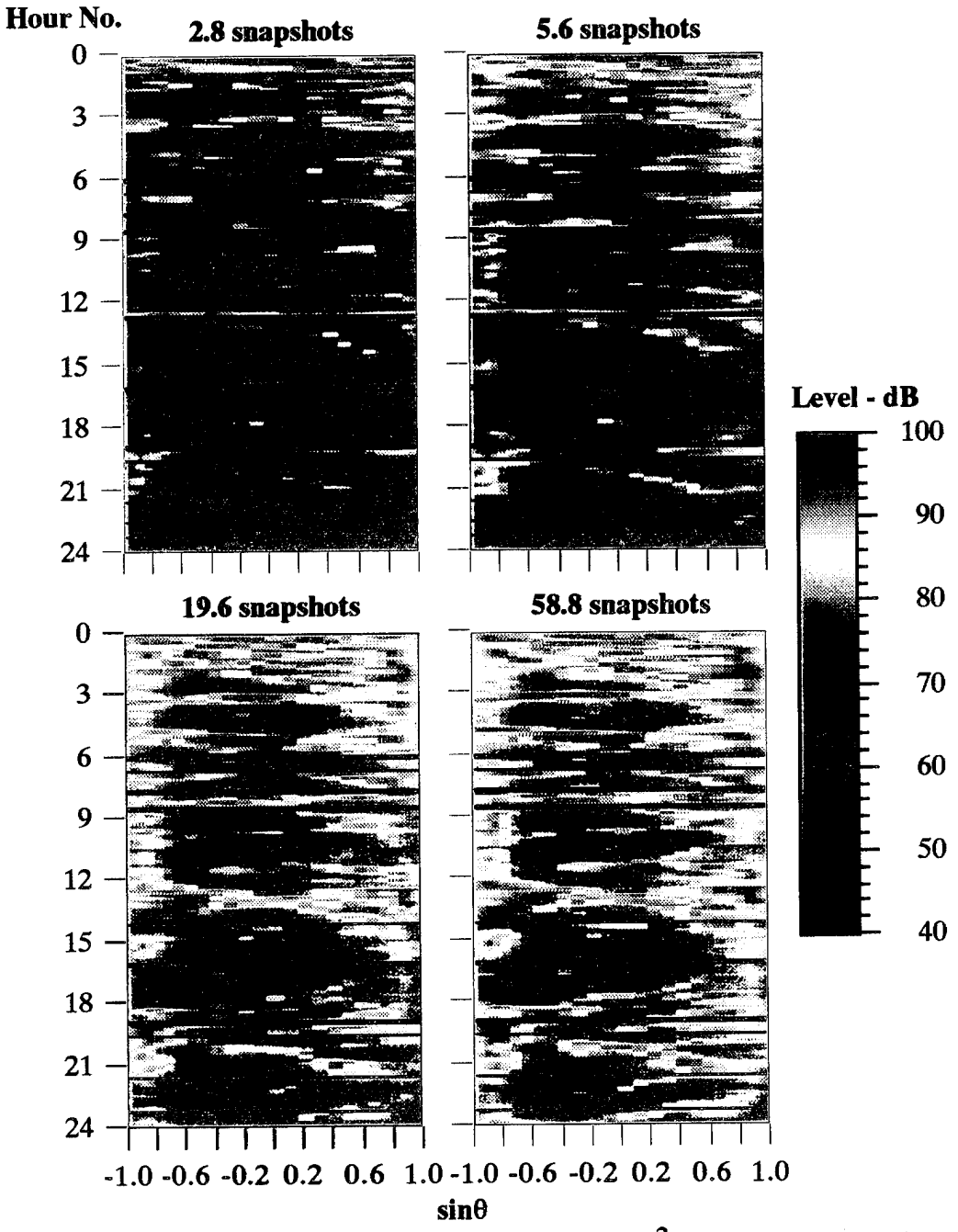

Figure 5.4 SWDS1 DMR beam noise with $D = 4$, $\sigma^2 = 0.005$, and $e = 0.5$.

AS-96-20

This page intentionally left blank.

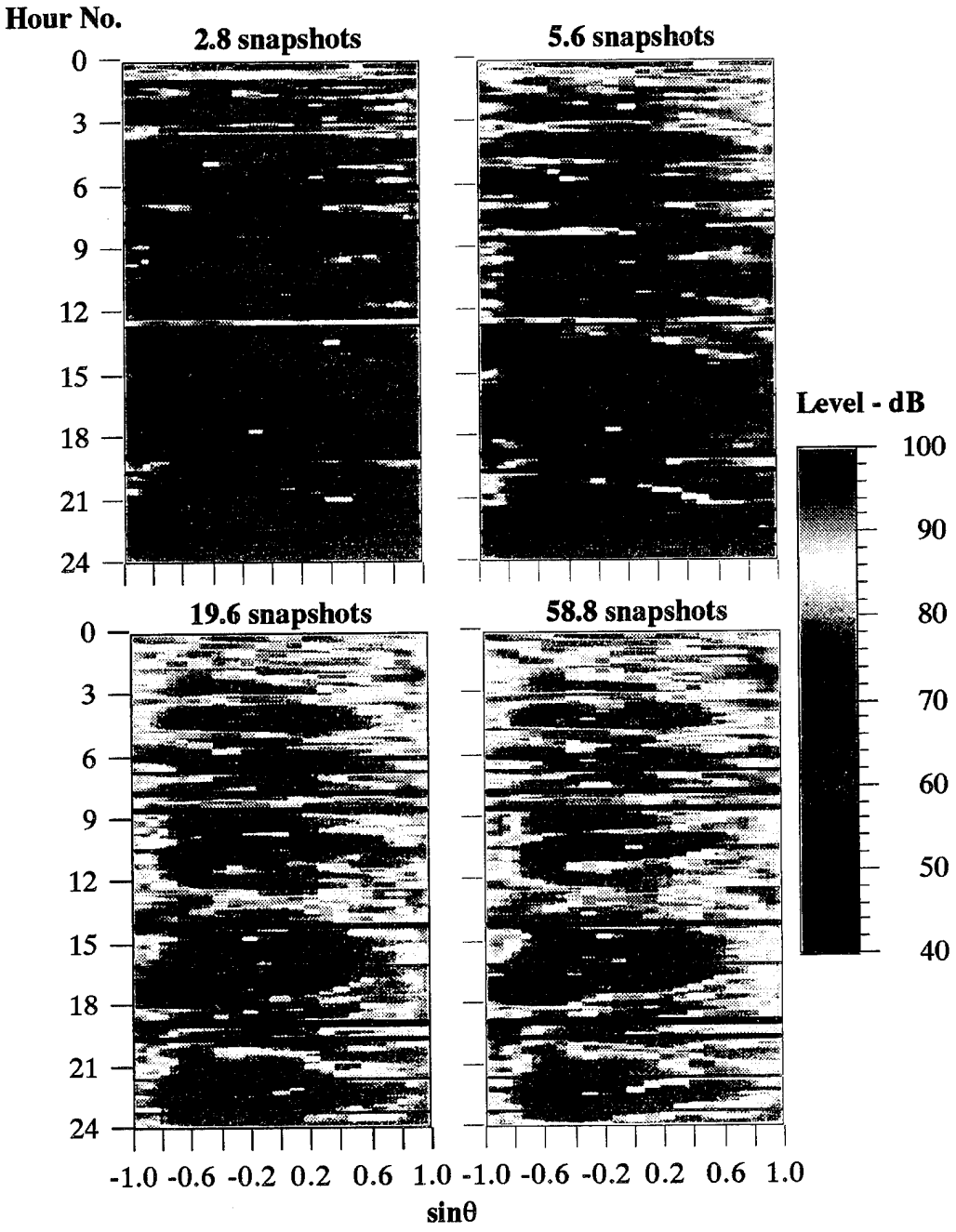

Figure 5.5 SWDS1 DMR beam noise with $D = 4$, $\sigma^2 = 0.005$, and $e = 1.0$.
AS-96-21

5.4 SWDS1 BEAM NOISE REDUCTION

As discussed in Section 1, Grant et al.[1] developed an expression of the MVDR beamformer output bias as a function of the number of snapshots. Figure 5.6 shows this expression assuming four and eight hydrophones in the CSM. Also plotted is the normalized median beam noise for the broadside beam from the standard adaptive beamformer and the DMR beamformer. In other words, the beam noise timeseries for the broadside beam for each case was extracted, and the median computed. The broadside beam was chosen because the beam noise is relatively quiet and the beam noise bias can be clearly seen in this area. Each noise value was normalized by the noise value for the 117.6 snapshot case, and the 117.6 snapshot cases were matched with the theoretical curve.

The results in Fig. 5.6 show that the ABF results fall with decreasing averages, as expected, but the DMR results are not quite as good as the theory suggests. WNGC ABF and MVDR were run using all eight eigenvalues of the CSMs, and the WNGC ABF and MVDR points follow the 8λ curve. The DMR beamformer was run using $D = 4$ eigenvalues; therefore the DMR points should follow the 4λ curve. However, the output power for the DMR data falls off faster than the 4λ curve and is closer to the 8λ curve. The plot above does show, however, that when the number of snapshots is less than 15, the DMR beamformer reduces the beam noise bias over MVDR and WNGC ABF.

5.5 SWDS1 SUMMARY

The SWDS1 analysis shows that the DMR beamformer reduces the beam noise bias for CSMs with low integration times when using either $e = 1.0$ or 0.5, and $\sigma^2 = 0.005$. Thus, more realistic performance estimates can be made with CSMs that have reduced integration times by using the DMR beamformer. The

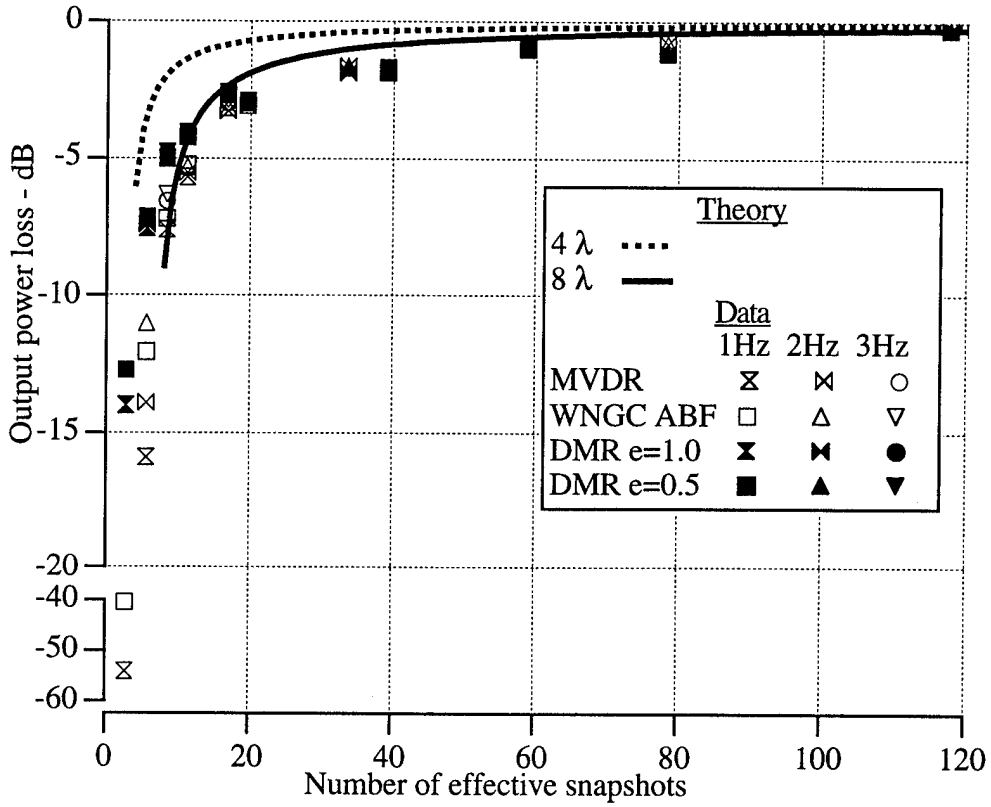

Figure 5.6 SWDS1 beam noise loss due to CSM averaging.

AS-96-22

estimated bias (based on the quiet-beam beam noise values) appears to increase faster than theory suggests for DMR, but the bias at very small CSM integration times is much smaller than that for the fully adaptive beamformer. Thus the DMR beamformer may have some attractive features for arrays with many elements that are deployed in highly dynamic noise environments, where shorter integration times may be needed.

This page intentionally left blank.

6. SHALLOW WATER DATA SET #2 RESULTS

There were only eight hydrophones in the first shallow water data set array. Therefore, the first shallow water data set was used to determine if the DMR beamformer could overcome the bias errors associated with standard adaptive beamformers when using CSMs with reduced integration times. Following this work, additional processing was performed on another shallow water data set. The second shallow water data set (SWDS2) array had 30 hydrophones and was used to determine the performance gain obtained by increasing the number of hydrophones. As the number of hydrophones in the array is increased, the integration time of the CSM must also be increased to keep the output power bias to reasonable levels. However, increasing the integration time of the CSM can "smear" the interferers, degrading beamformer performance. Confirming that this performance degradation does occur and determining whether the DMR beamformer can be used with shorter integration times to improve the beam noise degradation were the primary objectives in examining data from the second shallow water data set.

Initially, one period from the second shallow water data set was processed, and the results from this period will be examined in detail in Section 6.1. Once the results for this period were understood and verification that reasonable performance was being obtained from all the beamformers for all the cases, four additional periods were processed. These new results were combined with the results from the first period to add statistical significance to the overall results. The combined results are discussed in Section 6.2.

6.1 SWDS2 FIRST PERIOD

The first period for the SWDS2 contained 5.75 hours of data. Four sets of CSMs were calculated using the minimum integration time for the 8, 16, 24, and 30 hydrophone arrays discussed in Section 3.1.3. The CSMs were processed with the WNGC ABF. The WNGC ABF processes CSMs using a specified subset of hydrophones described by the CSM. The different combinations of the CSMs and the number of hydrophones used for beamforming are summarized in Table 6.1. The CSMs are designated by their integration times from Table 3.3. Shaded entries indicate cases that could not be processed because the integration time of the CSM is less than the minimum integration time required for the number of hydrophones. The checked entries are cases that were processed for this study. In addition to the ABF cases, the CSMs were processed using the DMR beamformer. Before determining which DMR cases could be processed, the appropriate values for D, as well as e and σ^2, were found. These values were chosen by examining the eigenvalues of the CSMs.

Table 6.1:
Shallow water data set #2 WNGC ABF and CBF processing cases.

Number of Hydrophones Processed	75 sec CSM	160 sec CSM	254 sec CSM	320 sec CSM
8	✓	✓		✓
16		✓		✓
24			✓	✓
30				✓

6.1.1 SWDS2 Eigenvalues and DMR Parameters

Figure 6.1 shows the eigenvalues of the 75 and 320 sec CSMs. Again, all the eigenvalues are scaled by the largest eigenvalue so that the largest eigenvalue is always 1, or 0 dB. Both CSMs have the same number of eigenvalues because all of the CSMs were created using 30 hydrophones.

Figure 6.1 shows that for most times, the last ten eigenvalues are very close to zero. Remember that the largest eigenvalues are associated with the loudest noise sources in the environment described by the CSM. This means that there are at most 20 dominant sources in the environment described by the CSM. Figure 6.1 also shows that the eigenvalues are similar for the 75 sec and the 30 sec CSMs. It is difficult to see much difference between the eigenvalues for the two CSMs. Therefore, to get a more detailed look at the eigenvalues, Fig. 6.2 shows the timeseries of the fifth, tenth, fifteenth, and twentieth eigenvalues for the 75 and 320 sec CSMs.

Again, the 75 sec CSM eigenvalues are close to the 320 sec CSM eigenvalues, but now it can be seen that the 75 sec CSM eigenvalues are $1-3$ dB lower than the 320 sec CSM eigenvalues. It is clear that the eigenvalues of the CSM depend only slightly on the integration time of the CSM. Therefore different values of D do not need to be chosen for the different CSMs. This makes sense as the environment described by the 75 and 320 sec CSMs is the same and the estimate of the largest eigenvalues should be the same if the integration time is sufficiently large.

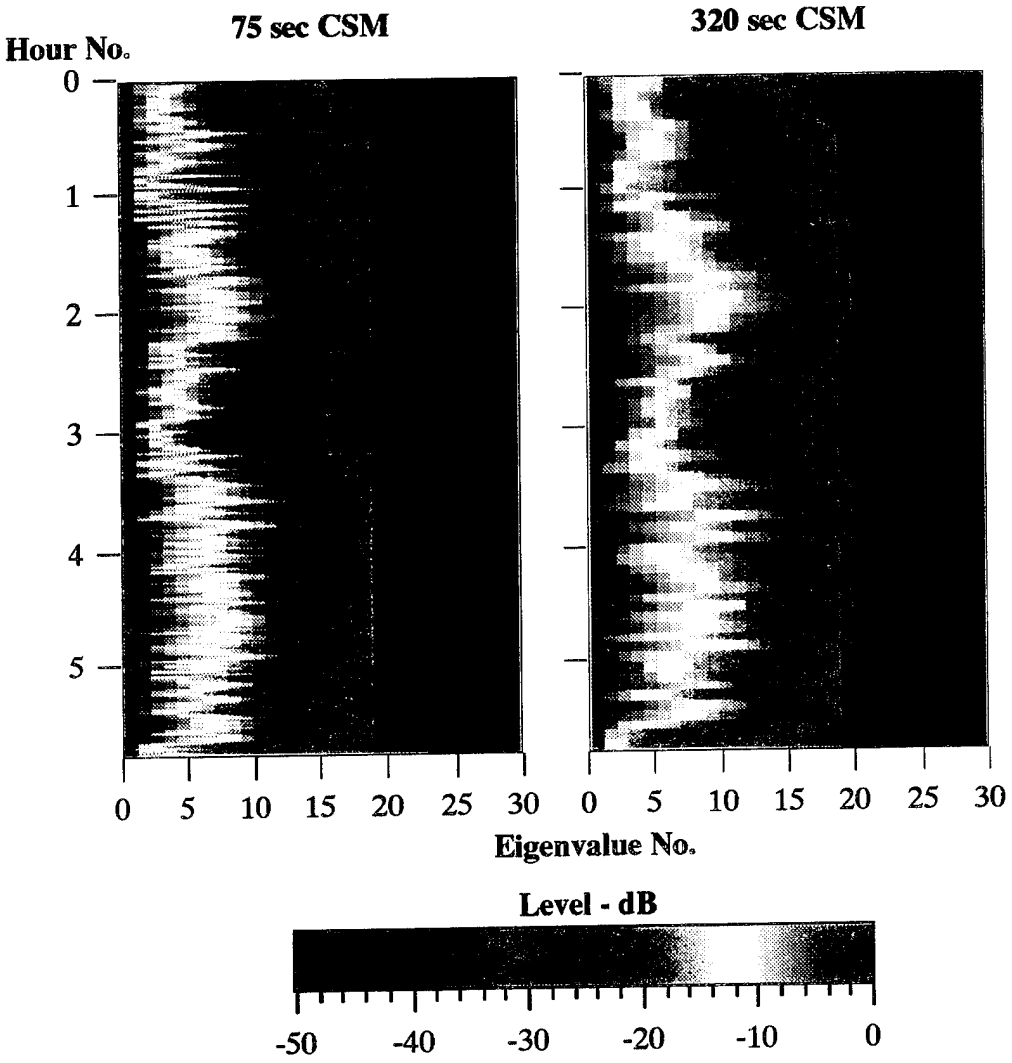

Figure 6.1 SWDS2 eigenvalues for the 75 and 320 sec CSMs.

AS-96-23

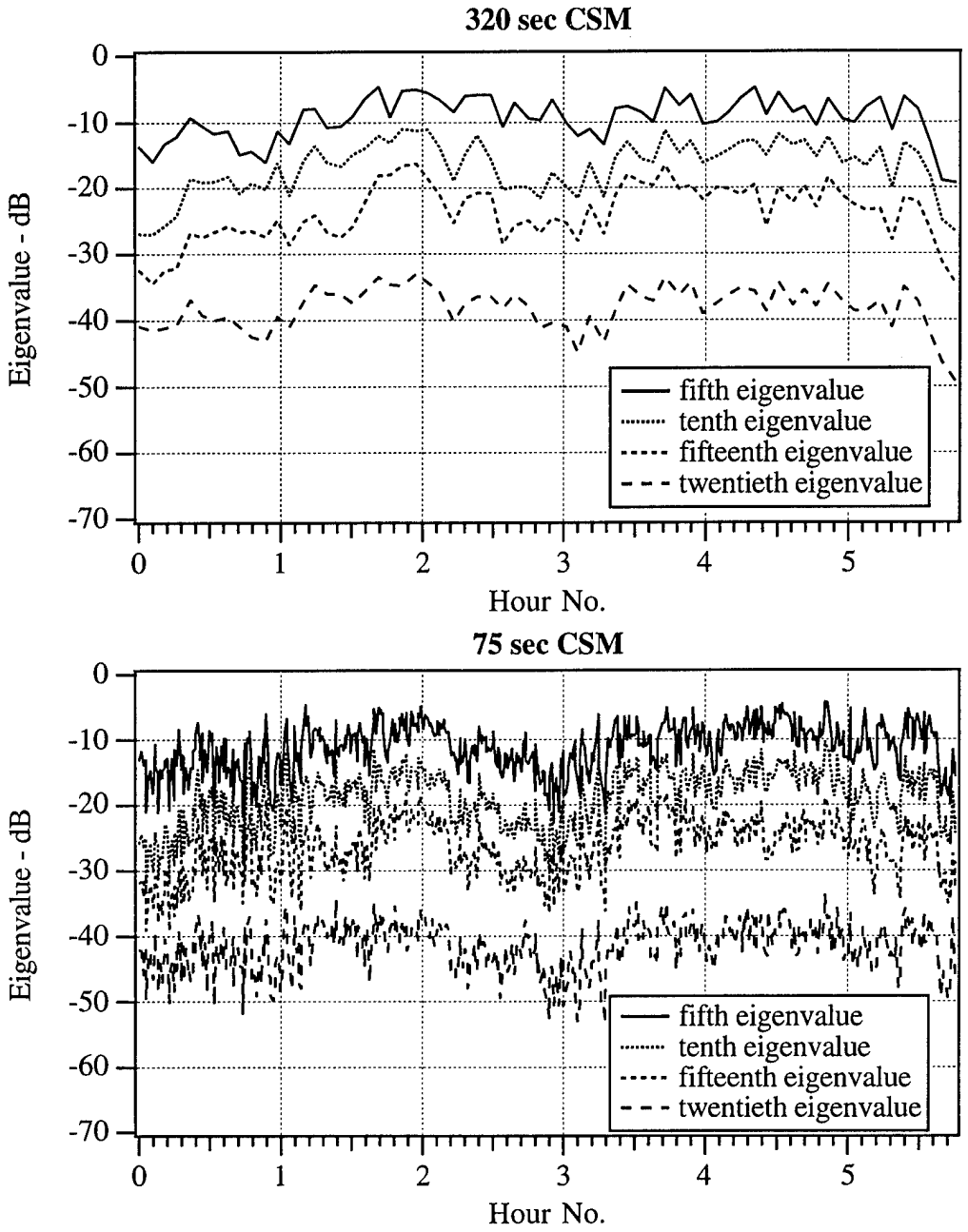

Figure 6.2 SWDS2 timeseries eigenvalues for the 75 and 320 sec CSMs.

AS-96-24

Figures 6.1 and 6.2 show that the first 15 or 16 eigenvalues contain the top 20 – 30 dB of the noise field, which is primarily due to the strongest interferers. Therefore σ^2 was chosen to be 0.001 to set the noise floor 30 dB below the first eigenvalue and near the sixteenth eigenvalue. Also, e was chosen to be 0.5 based on the previous study using the DWDS. Six different DMR cases were chosen to get a good idea of how the DMR beamformer performed with different values of D and the number of hydrophones processed. The different CSMs, the number of hydrophones processed, and the number of eigenvalues used in the DMR beamformer are listed in Table 6.2. After the ABF and DMR cases were chosen, the first period was processed with the WNGC and DMR beamformers.

Table 6.2:
Shallow water data set #2 DMR processing cases.

CSM Integration Time	Number of Hydrophones Processed	Number of Eigenvalues Processed, D
75 sec	16	8
75 sec	30	8
160 sec	30	8
160 sec	24	16
160 sec	30	16
254 sec	30	24

6.1.2 SWDS2 Beam Noise

Figure 6.3 shows the unshaded CBF and WNGC ABF beam noise for the 75 sec CSM processed with 8 hydrophones, the 160 sec CSM processed with 16 hydrophones, the 254 sec CSM processed with 24 hydrophones, and the 320 sec CSM processed with 30 hydrophones (the cases along the diagonal of

Table 6.1). The ABF noise levels are much quieter than the CBF noise levels in two areas of the plot: from hour 0 to hour 2 and $\sin\theta = -0.6$ to $\sin\theta = 0.2$ and from hour 4 to hour 5 and $\sin\theta = -0.2$ to $\sin\theta = 0.2$. This is because the adaptive beamformer nulls out the loud sources when the beamformer is steered in the quiet directions. The ABF noise levels are close to the CBF levels in the direction of the loud sources because the adaptive beamformer contains the white noise gain constraint that restricts mismatch losses.

The beam noise from the 75 sec CSM processed with eight hydrophones is unlike the beam noise for the rest of the CSMs. The loud sources in the 75 sec CSM beam noise are not as sharp as they sweep across the plot. This is because, as mentioned previously, the main lobe of the eight hydrophone beampattern is twice as wide as the main lobe of the other beampatterns. When the beamformer is steered near the loud sources, they are included in the main lobe of the eight hydrophone beampattern and are not attenuated. Thus, some of the energy of the loud sources appears in the beam next to the loud sources, making the beam noise look smoother.

Figure 6.3 also shows the difference in the beam noise due to the different CSM integration times. As the CSM integration time decreases, the sources look smoother because the integration time is sufficiently short to capture the dynamics of the noise field. For example, the loud source in the middle of the plot sweeps across approximately 5 degrees in one period in the 75 sec CSM beam noise (see point A), but the source sweeps across approximately 12 degrees in one period in the 320 sec CSM beam noise (see point B). This occurs because more CSM samples are averaged together to make one 320 sec CSM, and this "smears" the dynamics of the noise field.

Figure 6.4 shows another difference in the beam noise due to the different CSM integration times. Figure 6.4 shows the WNGC ABF quartile beam noise for the 75 sec CSM processed with 8 hydrophones, the 160 sec CSM processed with 16 hydrophones, and the 320 sec CSM processed with 30 hydrophones. The quartile beam contains the beam noise level such that 75% of the beam noise values are greater than that level for a given time period. The quartile beam is important because it is a measure of the quiet sector beam noise levels and hence shows the nulling performance of the ABF.

Figure 6.4 shows that the quartile beam noise decreases as the number of hydrophones increases. As seen in previous studies, the 16 hydrophone quartile beam noise is approximately 4 dB less than the 8 hydrophone quartile beam noise. The 30 hydrophone quartile beam noise is only 1 to 2 dB lower than the 16 hydrophone quartile beam noise. The 30 hydrophone array performs better because it has more degrees of freedom to null the interfering signals away from the look direction. However, the 30 hydrophone array does not achieve another 4 to 5 dB of gain over the 16 hydrophone array.

It is very interesting that the 30 hydrophone array does not produce a considerable increase of gain over the 16 hydrophone array. Thus, increasing the array size from 16 to 30 hydrophones may not be justified if using a fully adaptive algorithm. The 30 hydrophone array performance improvement is small because the 30 hydrophone array requires a longer integration time. Thus the interferers in the CSM appropriate for the 30 hydrophone array are smeared, requiring wider nulls. These wider nulls require more degrees of freedom; hence the 30 hydrophone does not produce a considerable increase of gain over the 16 hydrophone array.

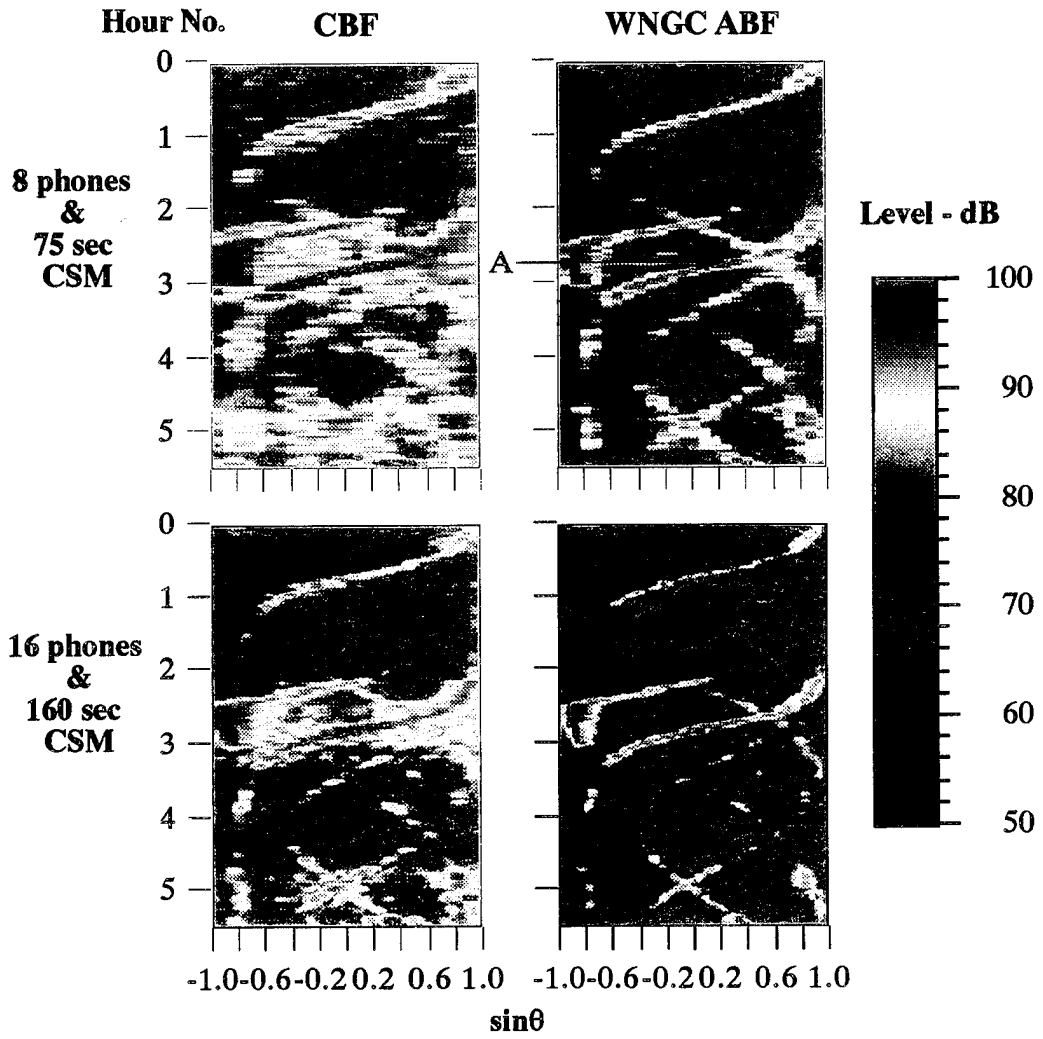

Figure 6.3 SWDS2 CBF and WNGC ABF beam noise.

AS-96-25

This page intentionally left blank.

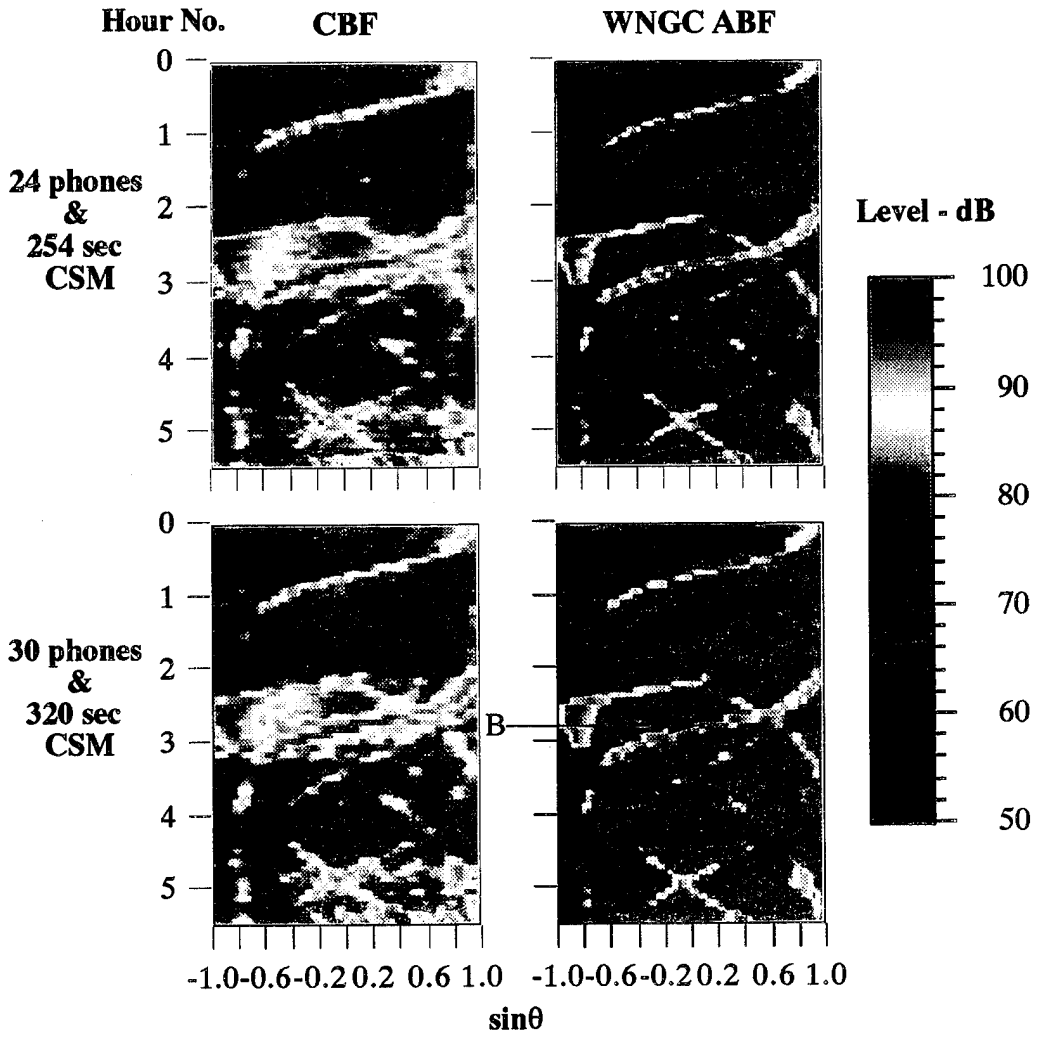

Figure 6.3 cont. SWDS2 CBF and WNGC ABF beam noise.

AS-96-26

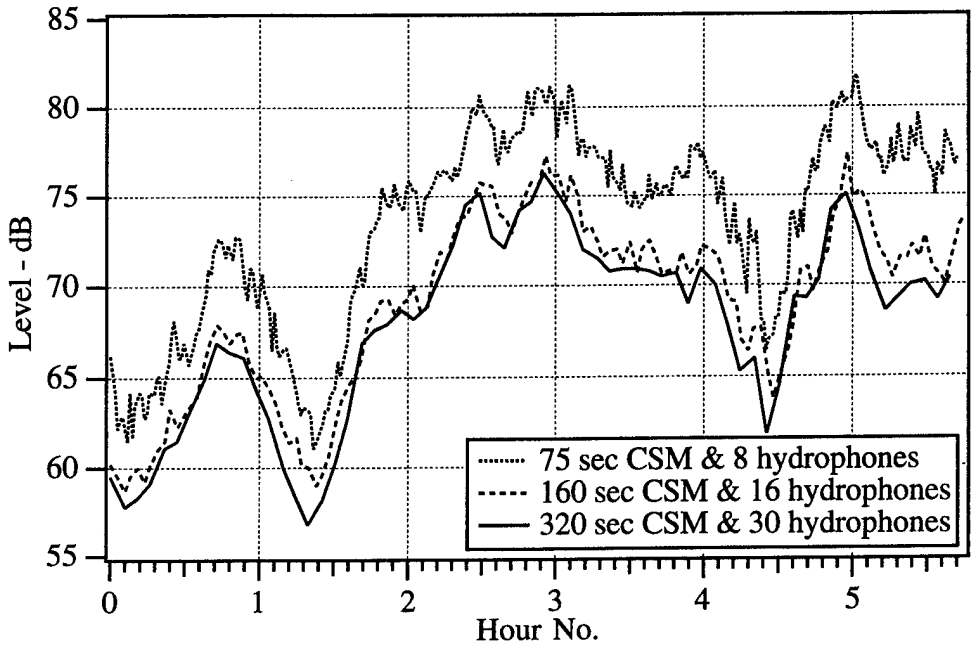

Figure 6.4 SWDS2 WNGC ABF quartile beam noise.

AS-96-27

Figure 6.5 shows the WNGC ABF quartile beam noise for the 160 and 320 sec CSMs. Both are processed with 16 hydrophones. Figure 6.5 shows the performance decrease due to the increase in CSM integration time. The 320 sec CSM has a longer integration time than the 160 sec CSM. Thus the interferers in the 320 sec CSM are smeared, requiring wider nulls. These wider nulls require more degrees of freedom; hence the beam noise using the 320 sec CSM is slightly higher at almost all times relative to the beam noise using the 160 sec CSM. Thus, the increased CSM integration time of the 320 sec CSM decreases the nulling performance of the beamformer.

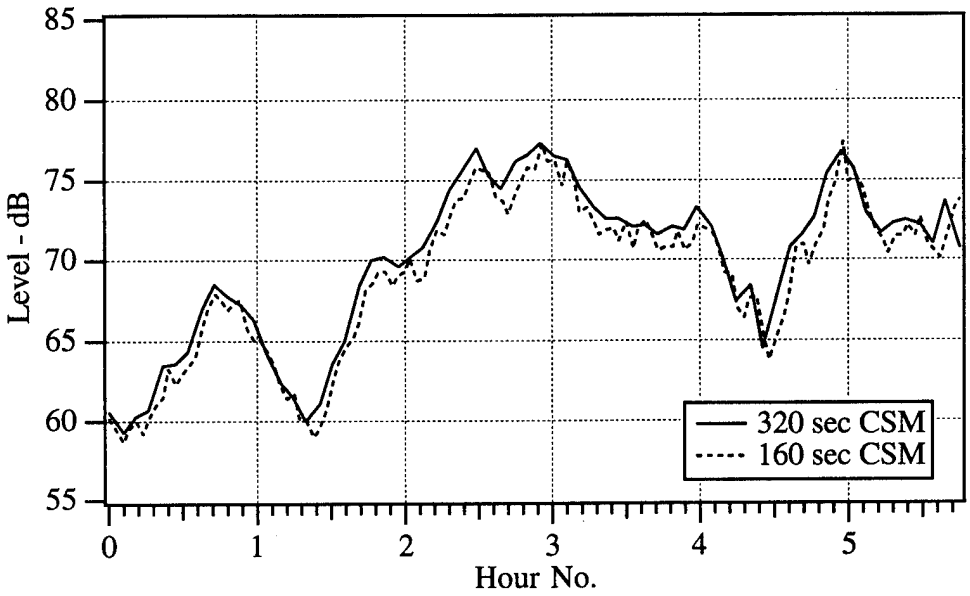

Figure 6.5 SWDS2 160 and 320 sec CSM WNGC ABF quartile beam noise using 16 hydrophones. AS-96-28

Figure 6.6 shows the DMR beam noise for the 160 sec CSM processed with 30 hydrophones and $D = 16$ and for the 75 sec CSM processed with 16 hydrophones and $D = 8$. The values of e and σ^2 used were 0.5 and 0.001, respectively. The beam noise plots for the other DMR cases from Table 6.2 processed with 16 and 24 eigenvalues are similar to the beam noise for the 160 sec CSM processed with 30 hydrophones and $D = 16$. The beam noise plots for the other DMR cases processed with 8 eigenvalues are similar to the beam noise for the 75 sec CSM processed with 16 hydrophones and $D = 8$.

Comparing the WNGC beam noise from Fig. 6.3 to the DMR beam noise from Fig. 6.6, the DMR beam noise looks almost the same as the WNGC beam noise with the 160 or 320 sec CSMs. The DMR beam noise has the same features as the WNGC beam noise, such as the loud sources that sweep across the middle of the plots and the quieter noise levels between $\sin\theta = -0.2$ and $\sin\theta = 0.2$. The

DMR beam noise levels are not as high as the WNGC ABF beam noise levels for the loud sources. This occurs because the DMR beamformer does not contain the white noise gain constraint. Therefore, the DMR beamformer can squint away from the loud sources.

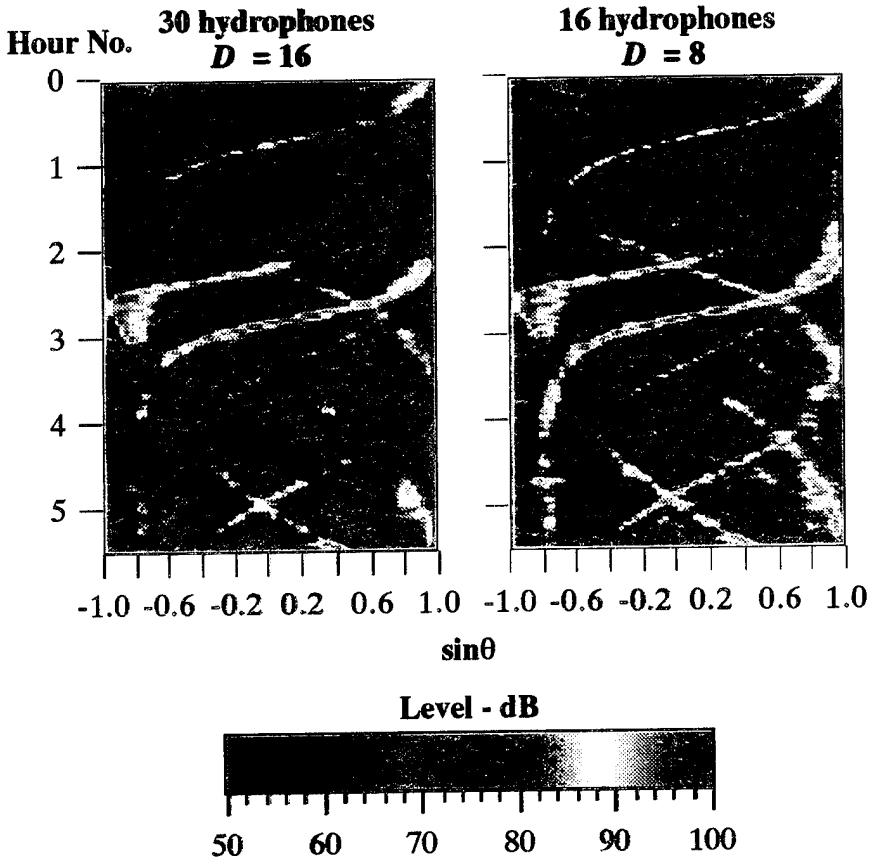

Figure 6.6 SWDS2 DMR beam noise processed with 30 hydrophones and $D = 16$ and with 16 hydrophones and $D = 8$.

AS-96-29

The beam noise for the DMR cases using eight eigenvalues is a little louder (in the quiet directions) than the beam noise for the other cases. However the eight eigenvalue DMR beam noise is much lower than the eight hydrophone WNGC beam noise from Fig. 6.3. This is interesting in that the 16 hydrophone, 8 eigen-

value DMR case shows significant improvement over the 8 hydrophone WNGC ABF case without any increase in CSM averaging or degrees of freedom. It is also interesting to note that the 16 hydrophone WNGC beamformer improves the beam noise a little more, but when using more than 16 eigenvalues (i.e. 16 eigenvalues/ 30 hydrophones, 24 eigenvalues/30 hydrophones, 30 eigenvalues/30 hydrophones), the improvement is minimal. This confirms that for this environment, increasing the number of eigenvalues beyond 16 does not provide a significant performance benefit.

The effect of the white noise gain can also be seen in Fig. 6.7. Figure 6.7 shows the broadside beam noise and white noise gain values for the DMR beamformer using 30 hydrophones and 16 eigenvalues. The broadside beam is perpendicular to the array line of bearing, corresponding to $\sin\theta = 0$. Figure 6.3 shows that the endfire, corresponding to $\sin\theta = 1$ or -1, beam noise values are always around 80 dB. However, the broadside beam noise ranges from 60 to 100 dB. The broadside beam was chosen because it contained a wide range of beam noise values and the white noise gain values for a wide range of beam noise values could be observed.

Recall that the white noise gain is a measure of the robustness of a beamformer and that small white noise gain values indicate that the beamformer is sensitive to mismatch. Figure 6.7 shows that the lowest white noise gain values are from times when the beam noise is loudest. Therefore, when the DMR beam noise is high, the beamformer is sensitive to mismatch errors and is probably attenuating the loud signal. Thus, the DMR beam noise is lower than the WNGC beam noise at the higher beam noise values.

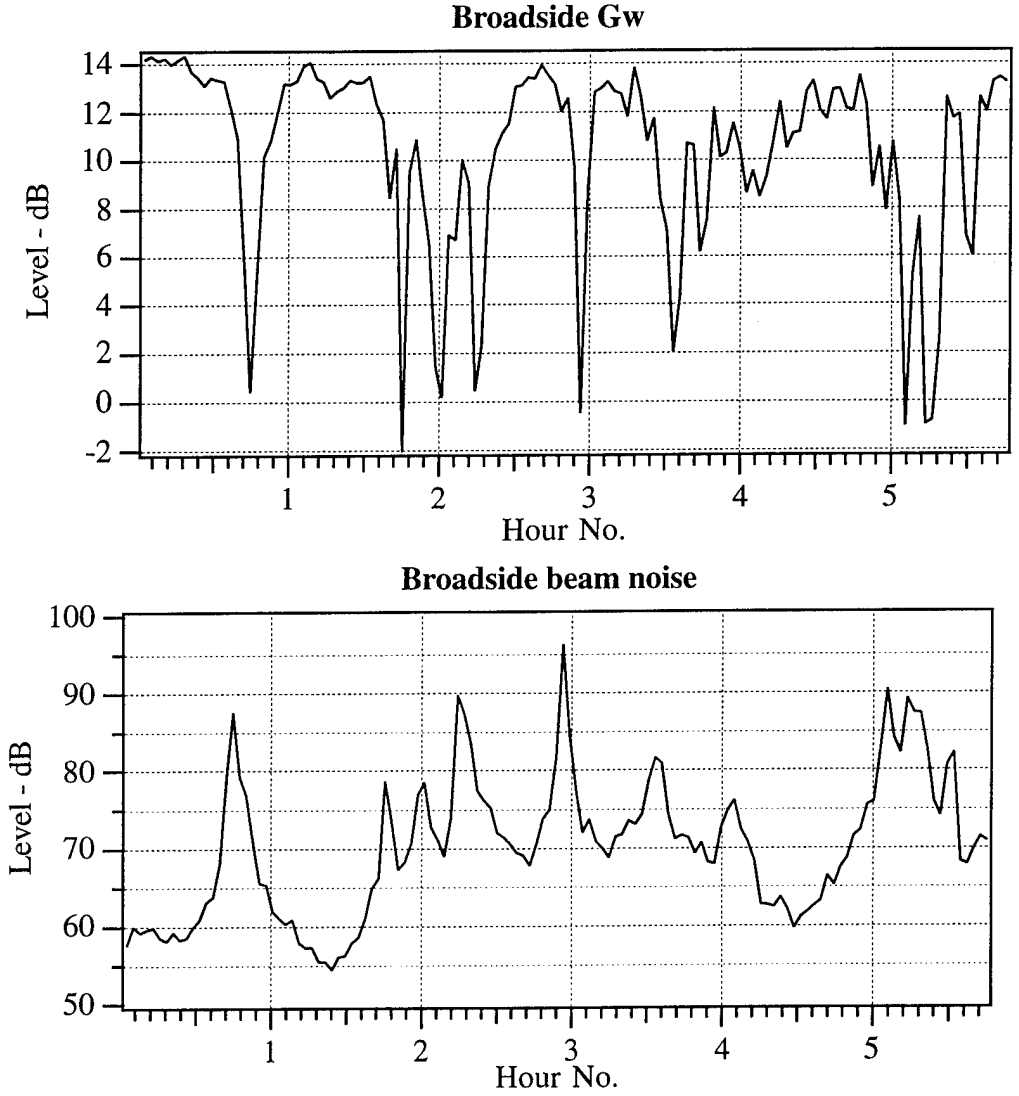

Figure 6.7 SWDS2 DMR broadside beam noise and white noise gain values using D = 16 and 30 hydrophones.

AS-96-30

To more easily compare the DMR beamformer with the WNGC beamformer, Fig. 6.8 shows the quartile beam noise from the two beamformers. Figure 6.8 shows the quartile beam noise for the 160 sec CSM processed with the WNGC beamformer using 16 hydrophones, the 160 sec CSM processed with the

DMR beamformer using 30 hydrophones and 16 eigenvalues, and the 320 sec CSM processed with the WNGC beamformer using 30 hydrophones.

Again the 30 hydrophone WNGC beamformer beam noise is 1–2 dB lower than the 16 hydrophones WNGC beamformer beam noise because the 30 hydrophone WNGC beamformer has more degrees of freedom to null out the interfering signals. For most periods, the DMR beamformer beam noise is also lower than the WNGC beamformer beam noise using 16 hydrophones. In fact the DMR beamformer beam noise is lower than the WNGC beamformer beam noise using 30 hydrophones for much of the time. Thus, the DMR beamformer using 30 hydrophones and 16 eigenvalues outperforms the WNGC beamformer using 30 hydrophones much of the time. This indicates that the 320 sec integration time is too long to capture the dynamics of this noise environment. Thus the DMR beamformer using the shorter CSM integration time (160 sec) can perform better than the WNGC beamformer using the longer integration time (320 sec).

The DMR beamformer uses a reduced rank estimate of the CSM. However the DMR beamformer performs as well as the WNGC beamformer with 30 hydrophones. This illustrates that all of the eigenvalues are not necessary to null the interfering signals and that a reduced rank beamformer may also be appropriate for this data set. Also, this performance is achieved using parameters very close to the parameters derived with the DWDS, again indicating that the DMR beamformer is relatively insensitive to the parameter setting.

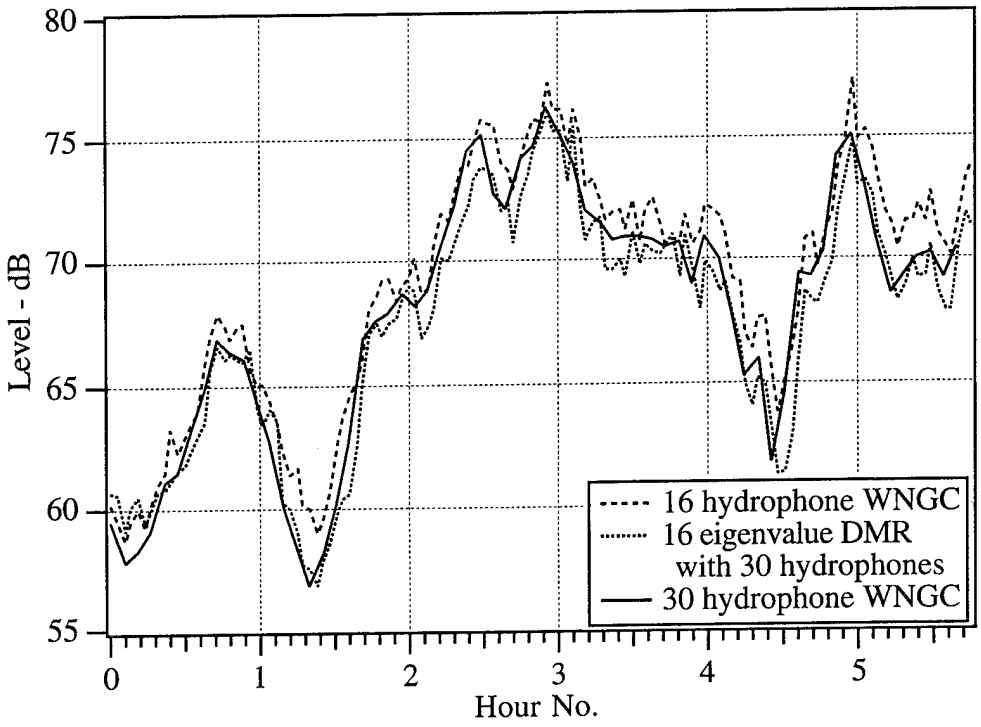

Figure 6.8 SWDS2 DMR and WNGC quartile beam noise.

AS-96-31

6.2 SWDS2 ALL PERIODS

After the first time period was processed and analyzed, five more periods were processed. Each of the new periods had approximately 5.75 hours of data so that slightly over 33 hours of data were processed. Only three array and beamformer combinations were processed on the new periods. The 160 sec CSM was processed with the WNGC beamformer using 16 hydrophones and with the DMR beamformer using 30 hydrophones and 16 eigenvalues. The 320 sec CSM was processed with the WNGC beamformer using 30 hydrophones. Recall that the 160 sec CSM integration time is sufficient for the 16 hydrophone array, whereas 320 sec are required for the 30 hydrophone array when both are processed with the WNGC beamformer.

Figure 6.9 shows the beam noise for the three cases and the six periods processed. The period analyzed in Section 6.1 is the second period in Fig. 6.9. All time periods were chosen because they contained a wide variety of beam noise values and characteristics. Period #1 has a very loud source that sweeps around the entire plot with a quiet region in the middle. Period #4 has another very loud source that sweeps across the plot and the rest of the beam noise is very quiet. Periods #3, #5, and #6 have many loud sources sweeping across the plots with quiet areas interspersed among the sources. It is clear from Fig. 6.9 that for a given period, the beam noise is similar for each processing case.

Again, the difference in the beam noise due to the different CSM integration times can be seen from Fig. 6.9. Recall that as the CSM integration time decreases, fewer CSM samples are averaged together. Thus, the sources look smoother in the 160 sec CSM beam noise because the integration time is sufficiently short to capture the dynamics of the noise field. For example, the loud sources in the plots sweep across fewer look directions in one period in the 16 hydrophone WNGC beam noise (points A) than in the 30 hydrophone WNGC beam noise (points B).

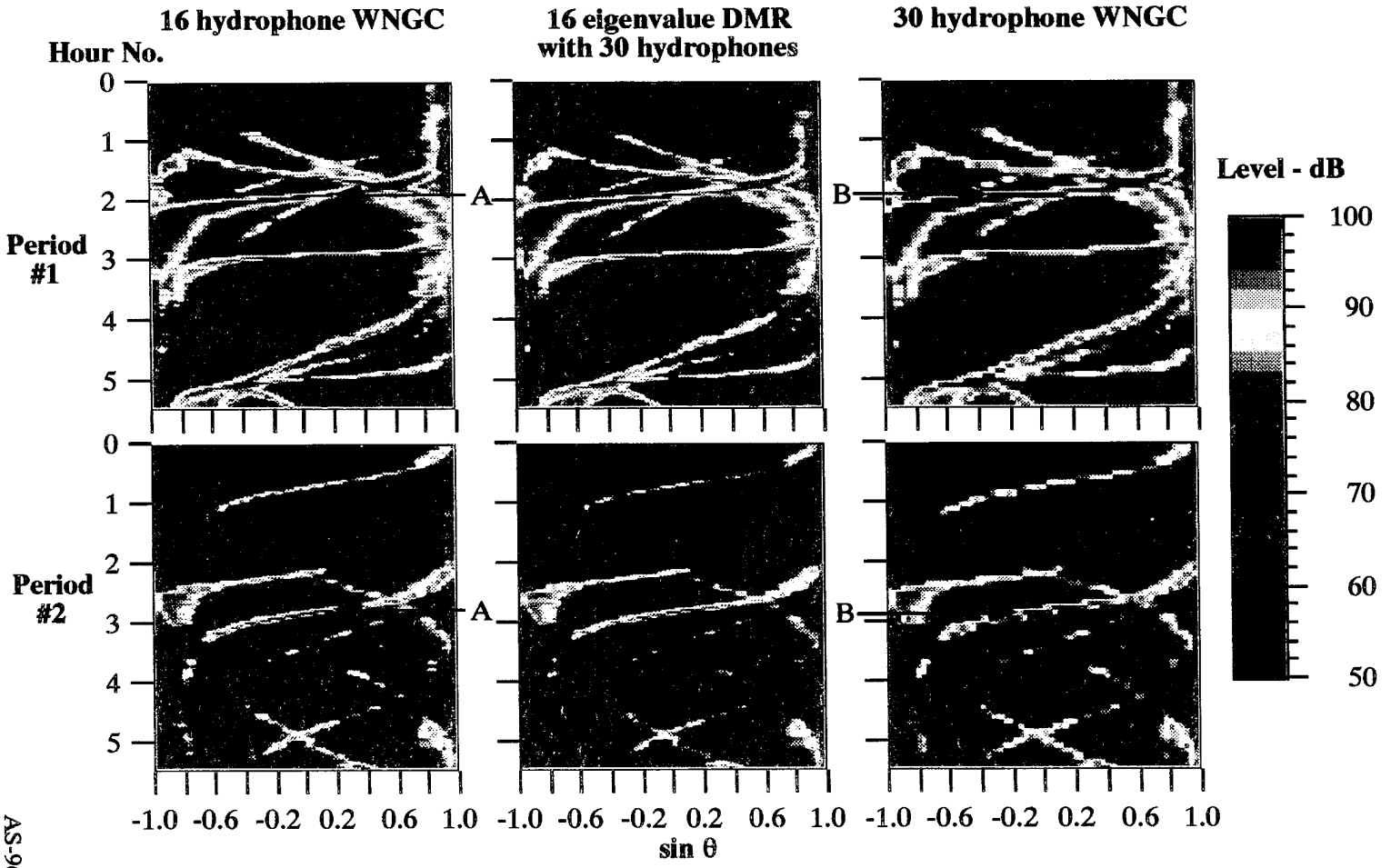

Figure 6.9 SWDS WNGC ABF and DMR beam noise for all periods (continued on following pages).

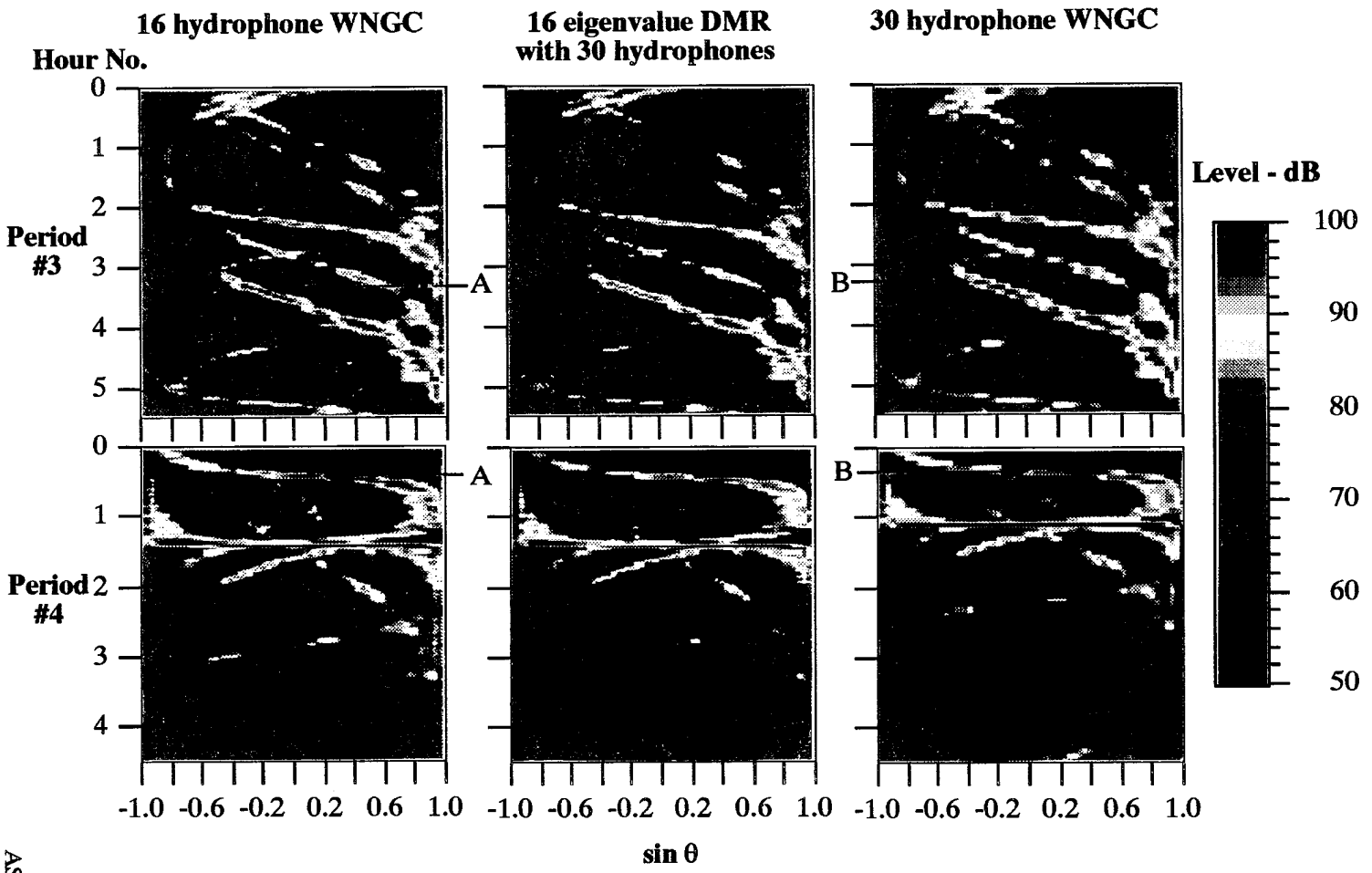

Figure 6.9 cont. SWDS WNGC ABF and DMR beam noise for all periods.

This page intentionally left blank.

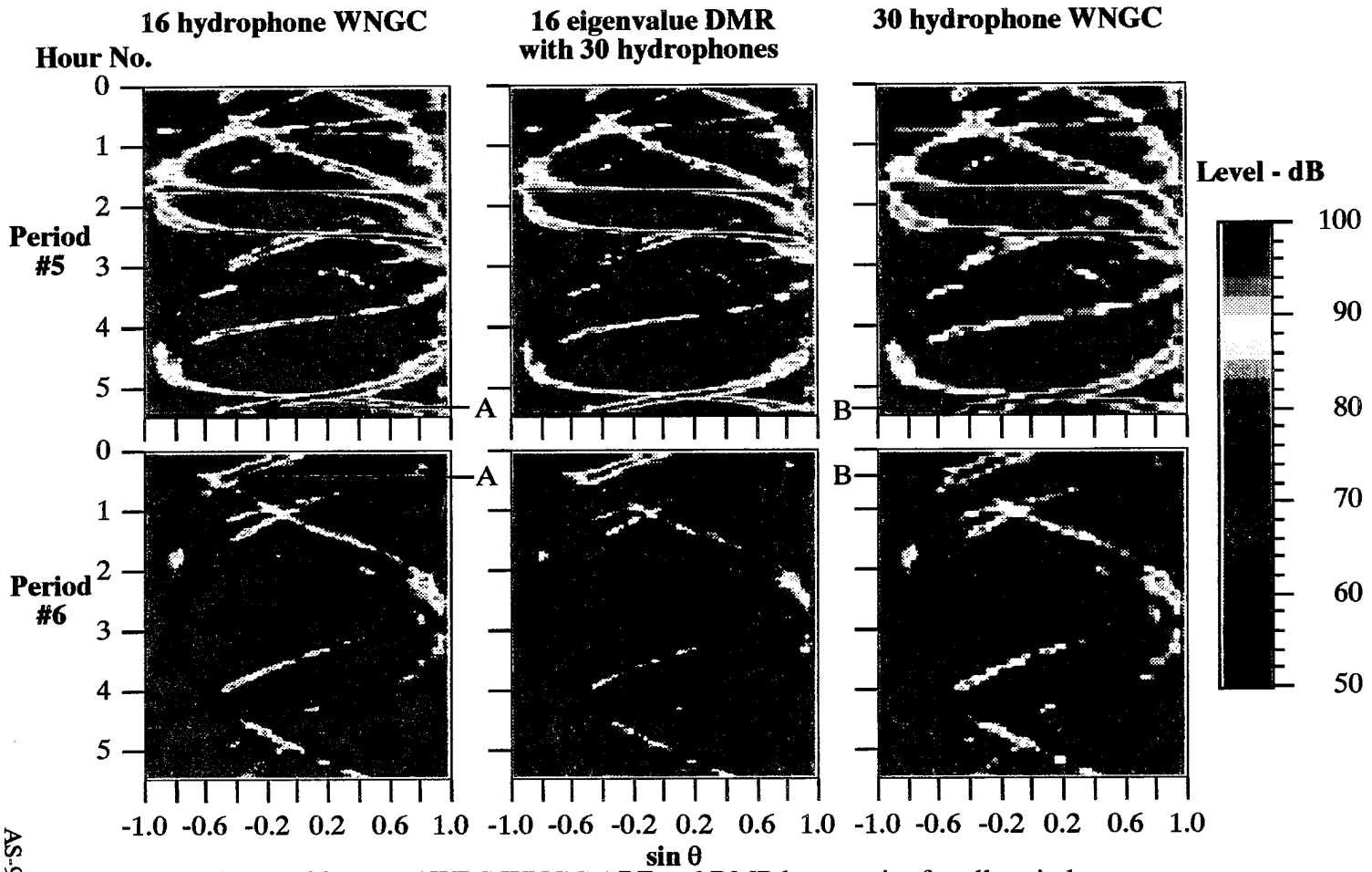

Figure 6.9 cont. SWDS WNGC ABF and DMR beam noise for all periods.

To see the difference between the cases in detail, Fig. 6.10 shows the cumulative distribution function (CDF) of the quartile beam noise for the same three cases. Again the results look similar for the three cases, but now it can be seen that the 30 hydrophone WNGC beam noise is lower than the 16 hydrophone WNGC case at almost all probability values. This is because the 30 hydrophone WNGC beamformer has more degrees of freedom to null out the interferers. Again, the WNGC beamformer with 30 hydrophones does not achieve a large increase of gain over the WNGC beamformer with 16 hydrophones. This occurs because the integration time of the CSM appropriate for the 30 hydrophone array is too long, causing the interferers to be smeared. The smeared interferers require wider nulls, and the wider nulls require more degrees of freedom.

In contrast, the DMR beamformer with 16 eigenvalues and 30 hydrophones performs better than the WNGC beamformer with 30 hydrophones. The 16 eigenvalue DMR beamformer beam noise is as low as the 30 hydrophone WNGC beam noise at most values and a little lower than the 30 hydrophone WNGC beamformer beam noise for some of the higher values. These higher values are caused by a loud interferer that sweeps across many look directions in one period. The DMR beamformer beam noise is lower than the 30 hydrophone WNGC beamformer beam noise at these values because the DMR beamformer uses CSMs with shorter integration times than the 30 hydrophone WNGC beamformer. The interferers in the CSMs with the shorter integration times are not as smeared. Thus, the nulls required for the interferers are smaller and require fewer degrees of freedom from the DMR beamformer. This allows the DMR beamformer to use any remaining degrees of freedom to lower the beam noise beyond the 30 hydrophone WNGC beam noise.

Thus for the entire time processed, the DMR beamformer with 30 hydrophones and 16 eigenvalues performs better than the 30 hydrophone WNGC beamformer. This performance is obtained with slightly more than half the number of eigenvalues and a significantly reduced CSM integration time. Thus, the DMR beamformer can achieve performance better than the WNGC beamformer with 30 hydrophones with essentially the same computational cost as the WNGC beamformer with 16 hydrophones.

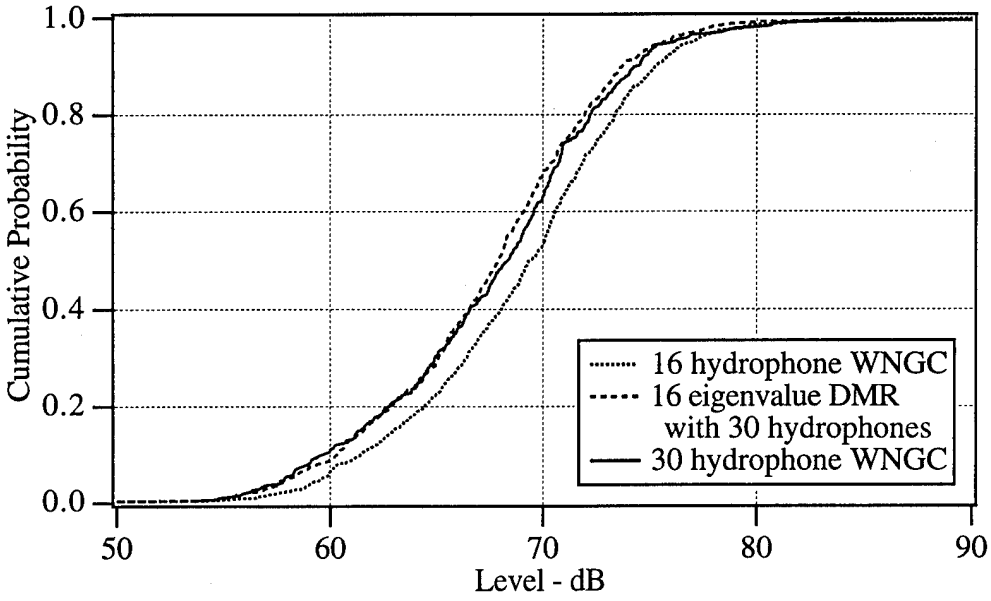

Figure 6.10 SWDS2 WNGC ABF and DMR quartile beam noise CDF for all periods.

AS-96-35

6.3 SWDS2 SUMMARY

The SWDS2 analysis shows many characteristics of the WNGC and DMR beamformers for CSMs with different integration times. First, CSMs were calculated with integration times of 75, 240, 160, and 320 sec. These times correspond to the minimum integration times for arrays with 8, 16, 24, and 30 hydrophones, respectively. The beampatterns of the four arrays were analyzed to determine the

number of beams to process and to show that beamformers with more hydrophones should perform better. The DMR parameters were chosen by looking at the eigenvalues of the CSMs, and σ^2 and e were almost identical to the values used with the previous data sets. The CSMs were processed with the WNGC and DMR beamformers, and the beam noise was analyzed.

The beam noise results showed that longer integration times decrease the WNGC ABF nulling performance when using the same number of hydrophones to process the CSM data. The smearing of the interferers due to long CSM integration times causes this decrease in performance. However, performance improvement still occurs when increasing the number of hydrophones. The SWDS2 analysis also showed that the DMR beamformer with 30 hydrophones and 16 eigenvalues performed almost as well as the WNGC beamformer with 30 hydrophones, both of which performed better than the WNGC beamformer with 16 hydrophones. The DMR beamformer does not contain the white noise gain constraint. Therefore the higher beam noise values were a little lower for the DMR beamformer than for the WNGC beamformer, but the difference was not significant.

Further work with other data is necessary to fully understand the potential advantages and performance improvements available with DMR. One issue that needs to be examined further is the sensitivity of the DMR beamformer to the number of eigenvalues chosen. However, this preliminary study indicates that using DMR for adaptive beamforming sonar applications is a feasible option.

7. CONCLUSIONS AND FUTURE WORK

7.1 SUMMARY AND CONCLUSIONS

The dominant mode rejection beamformer calculates adaptive weights based on a reduced rank CSM estimate, and appears to work as expected. The DWDS results determined initial values for the DMR parameters and showed that the performance of DMR beamformer is comparable to the fully adaptive WNGC beamformer. The performance of the DMR beamformer was significantly improved over CBF, with the exception of the period that no dominant noise sources existed. The values derived for the DMR parameters using the DWDS gave DMR beamformer performance close to the WNGC beamformer for the other data sets. Thus the DMR beamformer is not overly sensitive to these parameter values.

The SWDS1 results showed that DMR beamformer performance comparable to a fully adaptive beamformer could be achieved, without the penalties associated with the required increased integration time for the CSM. Further, the noise bias evident with the WNGC ABF and MVDR cases was noticeably reduced in the DMR results. Although the bias seen with DMR increased faster (with a reduction in integration time) than theory predicts, the bias reduction relative to the fully adaptive solution makes DMR attractive for highly dynamic noise environments where reduced integration times may be needed.

The SWDS2 results showed that WNGC ABF nulling performance increased as the number of hydrophones increased. As the number of hydrophones in the array is increased, the integration time of the CSM must also be increased to keep the output power bias to reasonable levels. However, the SWDS2 results

showed that increasing the CSM integration time while keeping the number of hydrophones in the beamformer array constant smeared the interferers, which slightly increased the beamformer beam noise. Finally, the SWDS2 results showed that the DMR beamformer with 30 hydrophones and 16 eigenvalues performed as well as the WNGC beamformer with 30 hydrophones and better than the WNGC beamformer with 16 hydrophones.

There are two potential advantages of the DMR beamformer over the WNGC beamformer that make the DMR beamformer more attractive. First, the computational burden required to process the 30 hydrophone WNGC ABF can be lessened by using the DMR beamformer. The WNGC beamformer must invert the entire CSM. The DMR beamformer avoids inverting the entire CSM and instead only requires estimates of the first D eigenvalues and eigenvectors. Hence, an algorithm to estimate the largest eigenvalues and eigenvectors of a matrix could be used with the DMR beamformer to substantially save computation time. The second advantage of the DMR beamformer is that the DMR beamformer with 30 hydrophones and 16 eigenvalues uses CSMs with lower integration times than the WNGC beamformer with 30 hydrophones. This allows the DMR beamformer to react faster to the environment described in the CSM.

7.2 SUGGESTIONS FOR FUTURE WORK

An issue that needs to be addressed further is determining the number of eigenvalues to use with the algorithm. The results showed that $e = 0.5$ works well and σ^2 values between 0.001 and 0.005 are appropriate. The sensitivity of the DMR beamformer's performance to the number of eigenvalues requires additional examination. Further, the relationship of the eigenvalues to the noise field should be examined also. This could be accomplished by looking at the conventional

beamformer results when using a reduced number of eigenvalues to form the CSM. This will provide insight as to how the performance deteriorates if the number of eigenvalues included in the solution is less than the number of dominant sources in the noise field. Finally, this study addresses only one reduced-rank beamformer. Other reduced-rank implementations should be examined to determine their relative merits and performance.

This page intentionally left blank.

REFERENCES

1. D. E. Grant, J. H. Gross, and M. Z. Lawrence, "Cross-Spectral Matrix Estimation Effects on Adaptive Beamforming," J. Acoust. Soc. Am. **98**, 517-524 (1995).

2. J. Capon and N. R. Goodman, "Probability Distributions for Estimates of the Frequency-Wavenumber Spectrum," *Proc. IEEE*, 1785-1786 (1970).

3. D. A. Abraham and N. L. Owsley, "Beamforming with Dominant Mode Rejection," Oceans 1990 Conference Proceedings, 470-475 (1990).

4. H. Cox, R. M. Zeskind, and M. M. Owen, "Robust Adaptive Beamforming," *IEEE Trans. Acoustics, Speech, and Signal Processing* **ASSP-35** (10), 1365-1376 (1987).

5. R. A. Gramann, "ABF Algorithms Implemented at ARL:UT," Applied Research Laboratories Technical Report No. 92-7 (ARL-TR-92-7), Applied Research Laboratories, The University of Texas at Austin, May 1992.

6. I. P. Kirsteins and D. W. Tufts, "Adaptive Detection Using Low Rank Approximation to a Data Matrix," *IEEE Trans. Aerospace and Electronic Systems* **30** (1), 55-67 (1994).

7. D. H. Johnson, and S. R. DeGraaf, "Improving the Resolution of Bearing in Passive Sonar Arrays by Eigenvalue Analysis," *IEEE Trans. Acoustics, Speech, and Signal Processing* **ASSP-30** (4), 638-647 (1982).

8. M. Kaveh and A. J. Barabell, "The Statistical Performance of the MUSIC and the Minimum-Norm Algorithms in Resolving Plane Waves in Noise," *IEEE Trans. Acoustics, Speech, and Signal Processing* **ASSP-34**, 331-341 (1986).

9. G. Bienvenu, and L. Kopp, "Optimality of High Resolution Array Processing Using the Eigensystem Approach," *IEEE Trans. Acoustics, Speech, and Signal Processing* **ASSP-31** (5), 1235-1247 (1983).

10. W. Chen, K. M. Wong, and J. P. Reilly, "Detection of the Number of Signals: A Predicted Eigen-Threshold Approach," *IEEE Trans. Signal Processing* **39** (5), 1088-1098 (1991).

11. D. A. Abraham, "Reduced Dimension Adaptive Beamforming," Technical Report No. 8747, Naval Underwater Systems Center, July 1990.

12. J. W. Kim, and C. K. Un, "A Robust Adaptive Array Based on Signal Subspace Approach," *IEEE Trans. Signal Processing* 41 (11), 3166-3171 (1993).

11 January 1996

DISTRIBUTION LIST
ARL-TR-96-2
Technical Report under Contract N00039-91-C-0082,
TD No. 01A2073, Acoustics and Engineering Analysis for ADS II

Copy No.

Commander
Space and Naval Warfare Systems Command
Department of the Navy
2451 Crystal Drive
Arlington, VA 22245-5200

1 Attn: CAPT W. Hatcher (PMW183)
2 R. Snuggs (PMW183T)
3 R. MacKinnon (PMW 183-11)
4 J. Feuillet (PMW183-12)
5 J. Thornton (PMW183-13)
6 LCDR J. Flayharty (PMW183-2)

Commanding Officer
Naval Command, Control, and Ocean Surveillance Center
RDT&E Division
53560 Hull Street
San Diego, CA 92152-5001

7 Attn: D. Barbour (712)
8 S. Whiteside (532)
9 J. Ehlers (7105)
10 N. Booth (541)
11 R. Harris

Office of the Chief of Naval Operations
Department of the Navy
Washington, DC 20350-2000

12 Attn: J. Schuster (N87T)
13 CAPT M. Wachendorf (N874)

Chief of Naval Operations
Naval Observatory
3450 Massachusetts Ave. N .W.
Washington, DC 20392-5421

14 Attn: E. Whitman (N096T)

Office of Naval Research
Department of the Navy
800 N. Quincy
Arlington, VA 22217-5660

15 Attn: J. DeCorpo (Code 32)
16 T. Goldsberry (Code 321US)
17 CDR M. Shipley (Code 321US)

Distribution List for ARL-TR-96-2 under Contract N00039-91-C-0082,
TD No. 01A2073
(cont'd)

Copy No.

Advanced Research Projects Agency
3701 N. Fairfax Dr.
Arlington, VA 22203-1714
18 Attn: W. Carey (MSTO)
19 T. Kooij (MSTO)
20 LCDR P. Feldmann

Director
Naval Research Laboratory
Washington, DC 20375-5000
21 Attn: S. Wolf (7120)
22 M. Czarnecki (5110)
23 M. Collins (Code 5160)
24 W. Smith (Code 5582)

Commanding Officer
Naval Air Warfare Center
Aircraft Division, Warminster
Warminster, PA 18974-5000
25 Attn: J. McEachern (Code 45C)
26 A. Horbach (Code 5031)

Officer in Charge
Naval Underwater Warfare Center
New London Detachment
New London, CT 06320-5594
27 Attn: N. Owsley

Director
Office of Naval Intelligence
4301 Suitland Rd.
Washington, DC 20395-5020
28 Attn: E. McWethy

29 Commanding Officer and Director
Defense Technical Information Center
8725 John J. Kingman Road, Suite 0944
Fort Belvoir, VA 22060-6218

30 Director
North Atlantic Treaty Organization
SACLANT ASW Research Centre
APO New York 09019
31 Attn: Library
32 D. Gingras

Distribution List for ARL-TR-96-2 under Contract N00039-91-C-0082,
TD No. 01A2073
(cont'd)

Copy No.

Marine Physical Laboratory
Scripps Institution of Oceanography
The University of California, San Diego
San Diego, CA 92132

33 Attn: W. Hodgkiss
34 G. D'Spain
35 W. A. Kuperman

The Johns Hopkins University
Applied Physics Laboratory
Johns Hopkins Road
Laurel, MD 20723-6099

36 Attn: K. McCann
37 R. Mitnick
38 H. South
39 B. Newhall

The Mitre Corporation
7525 Colshire Drive
McLean, VA 22102

40 Attn: K. Hawker
41 J. Hagy
42 R. Zeskind

Science Applications International Corporation
P.O. Box 1303
McLean, VA 22102

43 Attn: J. Hanna
44 R. Cavanagh

TRW, Inc.
Systems Integration Group
P.O Box 10400
Fairfax, VA 22031

45 Attn: L. Wood
46 B. Roman
47 C. Dabney

Digital System Resources
12450 Fair Lakes Circle, Suite500
Fairfax, VA 22203

48 Attn: B. Gallemore

Distribution List for ARL-TR-96-2 under Contract N00039-91-C-0082,
TD No. 01A2073
(cont'd)

Copy No.

	Applied Hydroacoustics Assn. 15825 Shady Grove Rd. #135 Rockville, MD 20850-4008
49	Attn: W. Allensworth
	AMRON Corporation 2001 Jefferson Davis Hwy #610 Arlington, VA 22202-3603
50	Attn: C. Christenson
	Alliant Techsystems Inc. 6500 Harbor Heights Parkway Mukilteo, WA 98275
51	Attn: N. Lehtomaki
52	Environmental Sciences Group, ARL:UT
53	Hans A. Baade, ARL:UT
54	Nancy R. Bedford, ARL:UT
55	Leon Brusniak, ARL:UT
56	Karl C. Focke, ARL:UT
57	David E. Grant, ARL:UT
58	Jonathan H. Gross, ARL:UT
59	David P. Knobles, ARL:UT
60	Robert A. Koch, ARL:UT
61	Thomas N. Lawrence, ARL:UT
62	Fredrick W. Machell, ARL:UT
63	Peter E. McCarty, ARL:UT
64	Clark S. Penrod, ARL:UT
65	Carol V. Sheppard, ARL:UT
66	Eric Smith, ARL:UT
67	Wade Trappe, ARL:UT

Distribution List for ARL-TR-96-2 under Contract N00039-91-C-0082,
TD No. 01A2073
(cont'd)

Copy No.	
68	Evan K. Westwood, ARL:UT
69–71	Tina R. Messerschmitt, ARL:UT
71–80	Richard A. Gramann, ARL:UT
81	Library, ARL:UT
82	Reserve, Environmental Sciences Group, ARL:UT